The structure and function of blue copper proteins

Ryde, Ulf; Olsson, Mats H M; Pierloot, Kristine

Published in:
Theoretical and Computational Chemistry

DOI:
10.1016/S1380-7323(01)80002-9

2001

Document Version:
Peer reviewed version (aka post-print)

The structure and function of blue copper proteins

Ulf Ryde[a], Mats H. M. Olsson[a], and Kristine Pierloot[b]*

[a]Department of Theoretical Chemistry, Lund University, Chemical Centre, P. O. Box 124, S-221 00 Lund, Sweden, e-mail: Ulf.Ryde@teokem.lu.se

[b]Department of Chemistry, University of Leuven, Celestijnenlaan 200F, B-3001 Heverlee-Leuven, Belgium

Theoretical investigations of the structure and function of the blue copper proteins and the dimeric Cu_A site are described. We have studied the optimum vacuum geometry of oxidised and reduced copper sites, the relative stability of trigonal and tetragonal Cu(II) structures, the relation between the structure and electronic spectra, the reorganisation energy, and reduction potentials. We also compare their electron-transfer properties with those of cytochromes and iron–sulphur clusters. Our calculations give no support to the suggestion that strain plays a significant role in the function of these proteins; on the contrary, our results show that the structures encountered in the proteins are close to their optimal vacuum geometries (within 7 kJ/mole) and that the favourable properties are achieved by an appropriate choice of ligands. We use the density functional B3LYP method for the geometries, multiconfigurational second-order perturbation theory (CASPT2) for calculations of accurate energies and spectra, point-charge models, continuum approaches, and combined classical and quantum chemical methods for the environment, and classical force-field calculations for estimation of dynamic effects and free energies.

1. INTRODUCTION

The blue copper proteins or cupredoxins are a group of proteins that exhibit a number of unusual properties, viz. a bright blue colour, a narrow hyperfine split-

*This investigation has been supported by grants from the Swedish Natural Science Research Council, the Flemish Science Foundation, the Concerted Action of the Flemish Government, and by the European Commission through the TMR program (grant ERBFMRXCT960079). It has also been supported by computer resources of the Swedish Council for Planning and Coordination of Research, Parallelldatorcentrum at the Royal Institute of Technology, Stockholm, the National Supercomputer Centre at the University of Linköping, the High Performance Computing Center North at the University of Umeå, and Lunarc at Lund University.

ting in the electron spin resonance (ESR) spectra, and high reduction potentials [1–3]. Moreover, crystal structures of these proteins show an extraordinary cupric geometry: The copper ion is bound to the protein in an approximate trigonal plane formed by a cysteine (Cys) thiolate group and two histidine (His) nitrogen atoms. The coordination sphere in most blue-copper sites is completed by one or two axial ligands, typically a methionine (Met) thioether group, but sometimes also a backbone carbonyl oxygen atom (in the azurins) or instead an amide oxygen atom from the side chain of glutamine (in the stellacyanins) [1–4].

The blue copper proteins serve as electron-transfer agents. Their distorted trigonal geometry is intermediate between the tetrahedral coordination preferred by Cu(I) and the tetragonal geometry of most Cu(II) complexes. As a result, the change in geometry when Cu(II) is reduced to Cu(I) is small [2,3,5], which gives a small reorganisation energy and allows for a high rate of electron transfer [6]. These unusual properties, unprecedented in the chemistry of small inorganic complexes, already in the 1960s led to the proposal that the protein forms a rigid structure, which forces the Cu(II) ion into a coordination geometry more similar to that preferred by Cu(I) [7,8]. These hypotheses were later extended into general theories for metalloproteins, suggesting that the protein forces the metal centre into a catalytically poised state, the entatic state theory [9,10] and the induced rack theory [11,12].

However, this suggestion has recently been challenged [13,14]. In particular, we have shown by quantum chemical calculations that the cupric geometry in the blue copper proteins is very close to the optimal vacuum structure of a Cu(II) ion with the same ligands [14]. Why then are the properties of the blue copper proteins so unusual, if not by protein strain? During the last five years, we have tried to answer this question using theoretical methods. In this review, we describe our results and discuss them in relation to the strain hypotheses. We also compare the blue copper proteins with related metal sites, such as the Cu_A dimer, cytochromes, and iron–sulphur clusters. Altogether, this gives an illustration of how theoretical methods, ranging from high-level quantum chemical calculations to pure classical simulations, can be used to study and solve biochemical problems.

2. METHODS

It is not yet possible to perform accurate quantum chemical calculations on a whole protein. Therefore models have to be constructed that are as realistic as possible but at the same time computationally tractable. We have used a number of techniques, ranging from high-level quantum chemical calculations on small models of the active site to classical simulations of the full protein. At the intermediate level, we have described the protein by quantum chemical methods and incorporated the effects of the surrounding protein and solvent by a variety of

methods, e.g. a point-charge model, a dielectric continuum, or by a classical force field. Each method has its strengths and disadvantages, and the choice of method is largely determined by the questions of interest and the available computer resources.

For quantum chemical geometry optimisations we have used the density functional method B3LYP, as implemented in the Mulliken, Turbomole, or Gaussian softwares [15–18]. Hybrid density functional methods have been shown to give as good or better geometries as correlated ab initio methods for first-row transition metal complexes [19–21], and the B3LYP method in particular seems to give the most reliable results among the widely available density functional methods [22]. In most calculations, we have used a basis set of double-ζ quality enhanced with *p*, *d*, and *f* functions for copper and iron [14,23,24] and the 6–31G* basis sets for the other atoms [25]. This basis set is denoted DZpdf/6–31G*.

For calculation of accurate energies, geometries, and electronic spectra, the CASSCF–CASPT2 approach was used (second order perturbation theory with a multiconfigurational reference state) [27]. This method has been shown to give reliable results for organic molecules as well as transition-metal complexes, with an error consistently less than 2500 cm^{-1} [28]. Generally contracted atomic natural orbitals (ANO) type basis sets were used in these calculations [29]. They have the virtue of being compact but at the same time optimised to include as much correlation as possible at a given size. Due to the size of the systems studied, basis sets of moderate size have been used, including up to *f*-type functions on Cu and a *d*-type function on S, but often no polarisation functions on C, N, and H.

The choice of the active orbital space for the CASSCF calculations is a crucial step, and has turned out to be especially difficult in these proteins and other systems containing a Cu–thiolate bond. From earlier studies it was known that in complexes with first-row transition metal ions with many 3*d* electrons, the active space should include one correlating orbital for each of the doubly occupied 3*d* orbitals [28]. Therefore the starting active space contains 10 orbitals (3*d* and 3*d*'). In addition, it is necessary to add the 3*p* orbitals on S_{Cys} to describe correctly the covalent character of the Cu–S_{Cys} bond and also 2*p* and 3*p* orbitals on nitrogen and sulphur to describe charge-transfer states. The final active space therefore contain 11 or 12 active orbitals (12 active orbitals are at present the upper limit for the CASPT2 method).

The CASSCF wavefunction is used as reference function in a second-order estimate of the remaining dynamical correlation effects. All valence electrons were correlated in this step and also the 3*s* and 3*p* shells on copper. Relativistic corrections (the Darwin and mass–velocity terms) were added to all CASPT2 energies. They were obtained at the CASSCF level using first-order perturbation theory. A level-shift (typically 0.3 Hartree) was added to the zeroth order Hamiltonian in order to remove intruder states [30]. Transition moments were computed with the CAS state-interaction method [31] at the CASSCF level. They were

combined with CASPT2 excitation energies to obtain oscillator strengths. The CASSCF–CASPT2 calculations were performed with the MOLCAS quantum chemistry software [32]. For further details, we refer to the original articles [14, 33–39].

In the quantum chemical calculations, only the copper ion and its ligands were included. Several models were tested for the ligands: histidine was modelled by either ammonia, imidazole (Im), or $ImCH_3$, cysteine by SH^-, SCH_3^-, or $SC_2H_5^-$, methionine by SH_2, $S(CH_3)_2$, or $S(CH_3)(CH_2CH_3)$, and amide ligands by formaldehyde, formamide, or acetamide. In the calculations on azurin, the main-chain linkage between the histidine ligand and the backbone amide group was also included in the calculations ($ImCH_2CH_2NHCOCH_3$). We have shown that a converged geometry and spectroscopy is obtained with imidazole as a model for histidine and with methyl groups on the sulphurs modelling cysteine and methionine [14,26,36]. Smaller models contain polar hydrogen atoms, which form artificial hydrogen bonds that may strongly distort the structure and change the energies. Fortunately, the explosive increase in computer power has the last two years made it unnecessary to compromise with the ligand models. However, before that, we often had to use smaller models and enforce symmetry to make the calculations feasible.

Naturally, calculations in vacuum cannot reproduce all the properties of a metal site in a protein. The simplest way to include the surroundings in quantum chemical calculations is to assign a charge to each atom in the protein (and possibly also an equilibrated ensemble of solvent molecules) and include the field of these charges in the calculations. This method was used in most of the calculations of electronic spectra [33,34,36,39]. The best available crystal structures were used as starting coordinates. Hydrogen atoms and solvent molecules (in the form of a spherical cap) were added and their positions were equilibrated by the Amber suite of programs [40]. The final coordinates were used in the spectra calculations together with charges from the Amber libraries [40].

Another method to include solvent effects in quantum chemical calculations is the continuum approach. In the polarised continuum method (PCM), a molecule is placed in a cavity formed by overlapping atom-centred spheres surrounded by a dielectric medium [41]. The induced polarisation of the surroundings is represented by point charges distributed on the surface of the cavity, and the field of these charges affects the wavefunction. Thus, solvation effects are included in the wavefunction in a self-consistent manner. In addition to this electrostatic term, the PCM method includes additional terms that affect only the solute energy, viz. cavitation, dispersion and exchange energy [42]. We have used the conductor or self-consistent isodensity PCM methods [43,44] as implemented in the Gaussian 98 software [17]. Further details are given in the original references [35,45].

Continuum methods can also be used in classical calculations including the full protein. In such calculations, each atom in the protein is assigned a point charge.

For the active site, the charge may be taken from a quantum chemical calculation [46]. Moreover, the protein is assigned a low dielectric constant (typically 4), whereas the surrounding solvent is assigned the value of water (~80). Then, the Poisson–Boltzmann equation is solved numerically on a grid covering the protein and parts of the solvent [47]. Naturally, this method is less accurate than the PCM, but it can be used for much larger systems. We have used this method as implemented in the MEAD software [48] for the calculation of reduction potentials [45,49]. A related method is the protein-dipole Langevin-dipole method, in which water molecules are represented by Langevin dipoles on a grid and polarisation effects are included [50]. It has successfully been used in several investigations of the reorganisation energy and reduction potentials of proteins [50–53], but we have only used it in some explorative calculations.

We have run several types of classical simulations on blue copper proteins, e.g. energy minimisations, molecular dynamics simulations, free energy calculation, and potential of mean force computations [33,34,36,38,39,54], all with the Amber software [40]. In such calculations, the copper ion and its ligands pose a special problem, since they are not included in the force fields. For crude calculations (especially when the metal site is kept fixed), it may be sufficient to determine an appropriate set of charges for the copper ion and its ligands from a fit to the electrostatic potential calculated by quantum chemical methods [46] (there is a significant transfer of charge from the ligands to the copper ion). For more accurate calculations, a full force-field parameterisation of the copper ion and its ligands has to be performed, involving charges, force constants, and equilibrium parameters. We have performed such a parameterisation for the copper sites in oxidised and reduced plastocyanin and oxidised nitrite reductase (both the type 1 and type 2 copper sites) [54].

The most satisfactory way to include the effect of the surroundings in quantum chemical calculations is to combine a quantum chemical and a classical program, the QC/MM approach. In this method, the interesting part of the system is treated by quantum chemical methods, whereas the rest is treated by classical methods. Classical forces on the quantum atoms are added to the quantum chemical forces before the atoms are moved (either in a geometry optimisation or in molecular dynamics simulations). If there are bonds between the quantum chemical and classical systems, special action is taken. This approach is very popular at present, and many different variants have been suggested [55–60]. We have recently updated our QC/MM program COMQUM [57] to incorporate the density functional methods of Turbomole [16] and the accurate force field methods in Amber [40]. This program has been used to optimise the geometry of the copper site in three blue copper proteins, to estimate strain energies, and to calculate reorganisation energies [26].

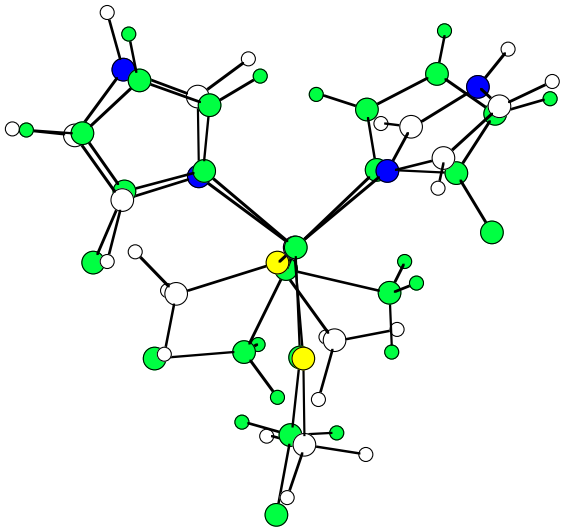

Figure 1. A comparison of the optimised structure of $Cu(Im)_2(SCH_3)(S(CH_3)_2)^+$ [14] and the crystal structure of plastocyanin (shaded) [4].

3. GEOMETRY

3.1 The optimal geometry of the blue-copper active site

According to the induced-rack and the entatic state hypotheses [10,12], the Cu(II) coordination sphere in the blue copper proteins is strained into a Cu(I)-like structure. Such hypotheses are hard to test experimentally, but with theoretical methods it is quite straightforward. The actual coordination preferences of the copper ion can be determined by optimising the geometry of the ion and its ligands in vacuum; if the optimised structure is almost the same as in the proteins, strain is probably of minor importance for the geometry.

We have optimised the geometry of $Cu(Im)_2(SCH_3)(S(CH_3)_2)^+$, a realistic model of the oxidised prototypical $CuHis_2CysMet$ blue-copper site (e.g. in plastocyanin), using the density functional B3LYP method [14]. The result is sensational but convincing. As can be seen in Figure 1 and Table 1, the optimised geometry is virtually identical to the one observed experimentally in the blue copper proteins. Almost all bond lengths and bond angles around the copper ion are within the range observed in crystal structures, and most of them are close to the average values for the proteins. Only two small, but significant, differences can be observed: a slightly too long $Cu–S_{Cys}$ bond and a slightly too short $Cu–S_{Met}$ bond. These differences can be fully explained by the dynamics of the system, which increase the average $Cu–S_{Met}$ bond length by at least 10 pm [54], and by deficiencies in the theoretical method (the more accurate CASPT2 method, gives a 7 pm shorter $Cu–S_{Cys}$ bond and a 7 pm longer $C–S_{Met}$ bond [14]).

Equally convincing results have been obtained for the optimal structure of $Cu(Im)_2(SCH_3)(OCCH_3NH_2)^+$, a model of the ligand sphere of oxidised stellacyanin [33], as is also shown in Table 1. It should be noted that no information

Table 1. Comparison of the geometry of optimised models and crystal structures of blue copper proteins [14,34,54]. *Ax* is the axial ligand and φ the angle between the S_{Cys}–Cu–*Ax* and N–Cu–N planes.

Model	Distance to Cu (pm)			Angle subtended at Cu (°)				φ
	S_{Cys}	N	*Ax*	N–N	S_{Cys} –N	S_{Cys}–*Ax*	N–*Ax*	
$Cu(Im)_2(SCH_3)(S(CH_3)_2)^{+a}$	218	204	267	103	120–122	116	94–95	90
Plastocyanin oxidised	207–221	189–222	278–291	96–104	112–144	102–110	85–108	77–89
$Cu(Im)_2(SCH_3)(S(CH_3)_2)^{+}$	232	214–215	237	109	105–108	115	107–113	89
$Cu(Im)_2(SCH_3)(S(CH_3)_2)^{+b}$	227	205–210	290	119	112–120	99	100–101	88
Plastocyanin reduced	211–217	203–239	287–291	91–118	110–141	99–114	83–110	74–80
$Cu(Im)_2(SH)(S(CH_3)_2)^{+c}$	223	205–206	242	100	97–141	103	95–126	62
Nitrite reductase oxidised	208–223	193–222	246–270	96–102	98–140	103–109	84–138	56–65
$Cu(Im)_2(SCH_3)(OCCH_3NH_2)^{+a}$	217	202–206	224	103	122–125	113	92–95	88
Stellacyanin oxidised	211–218	191–206	221–227	97–105	116–141	101–107	87–102	82–86

[a] Trigonal structure
[b] The Cu–S_{Met} bond length was constrained to 290 pm.
[c] Tetragonal structure

from the crystal structures has been used to obtain these structures; they are entirely an effect of the chemical preferences of the copper ion and its four ligands. Thus, the cupric structure in the oxidised blue copper proteins is clearly neither unnatural nor strained.

Geometry optimisations of the corresponding reduced models are more complicated, because the lower charge on the copper ion leads to weaker bonds, so that the geometry of the complex is very sensitive to electrostatic interactions with the surrounding protein (e.g. hydrogen bonds) [14]. The optimum vacuum structure of the $Cu(Im)_2(SCH_3)(S(CH_3)_2)$ complex is more tetrahedral than the active site in reduced plastocyanin and it has a short Cu–S_{Met} bond (237 pm, see Table 1) [14]. However, the potential surface of the Cu–S_{Met} bond is extremely flat (c.f. Figure 10). If this bond length is fixed at the crystal value (290 pm) and the complex is reoptimised, a structure is obtained that is virtually identical to the crystal structure of reduced plastocyanin. Interestingly, this structure is only 4 kJ/mole less stable than the optimal tetrahedral structure, which is within the error limits of the method [14]. Moreover, many effects not included in these calculations tend to elongate this bond (see below). Thus, we cannot decide whether the reduced structure is slightly distorted by the protein or not, but it is clear that the energy involved is extremely small.

We have also studied the structure of azurin [37,61]. In this protein there is another weak axial ligand of the copper ion, a backbone carbonyl group. This group is chemically similar to the amide oxygen ligand in stellacyanin. Therefore, it is not surprising that it prefers to bind to copper at a rather short distance, about 230 pm for the $Cu(Im)(ImCH_2CH_2NHCOCH_3)(SCH_3)(S(CH_3)_2)^+$ model, similar to the Cu–O distance in stellacyanin. However, it costs less than 6 kJ/mole to move it to the distance found in the crystal structure (around 310 pm, see Figure 2). The same applies to the methionine ligand. It prefers to bind in the second sphere of the complex, but it also has a shallow minimum around 290 pm, which is only 3 kJ/mole higher in energy. The reduced site behaves similarly [61].

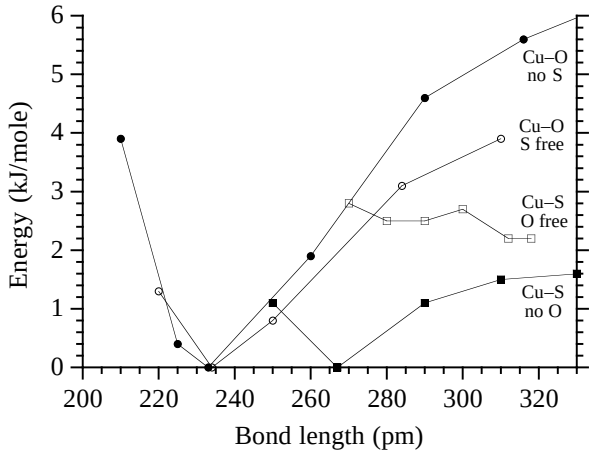

Figure 2. Potential surfaces for the Cu–O and Cu–S_{Met} bonds in three models of oxidised azurin. "No S" and "no O" refer to the $Cu(Im)(ImCH_2CH_2NHCOCH_3)(SCH_3)^+$ and $Cu(Im)_2(SCH_3)(S(CH_3)_2)^+$ models, respectively, whereas the other two curves were obtained with the $Cu(Im)(ImCH_2CH_2NHCOCH_3)(SCH_3)(S(CH_3)_2)^+$ model with the Cu–O or Cu–S_{Met} bond at its equilibrium distance [37].

Interestingly, if the copper ion in azurin is replaced by Co(II), things change drastically, as can be seen in Figure 3. If one of the axial ligands is removed, the other binds strongly to the metal ion, with a force constant of the same size as for the equatorial ligands and about six times larger than those of the Cu(II) complex. The optimum Co–O and Co–S_{Met} distances are 207 and 243 pm, respectively. The potential surface for the carbonyl ligand is not changed much if the methionine ligand is added; cobalt still prefers a short Co–O bond by about 30 kJ/mole over the distance found in the copper protein, which explains the short distance in the crystal structure (~220 pm) [62]. However, if the Co–O distance is fixed at the crystal value, the Co–S_{Met} potential change strongly: The methionine model prefers to bind in the second sphere, but the surface becomes extremely flat, so flat that the Co–S_{Met} bond length can be varied between 280 and 380 pm at a cost of less than 1 kJ/mole. In the crystal structure it is 340–370 pm.

Thus, the cobalt site is four-coordinate with a strong bond to the carbonyl group, whereas the copper site is effectively three-coordinate. The bonds to the other axial ligands are determined by interactions with the protein, rather than with the metal. The only way to study such weak bonds in vacuum models is by studying the potential surfaces, such as those in Figures 2 and 3.

3.2. Trigonal and tetragonal Cu(II) structures

Why does a Cu(II) ion with the ligands in the blue copper proteins assume a trigonal structure, whereas most inorganic cupric complexes are tetragonal (square planar, square pyramidal, or distorted octahedral) [63,64]? We have faced this question by optimising the geometry of a number of models of the type

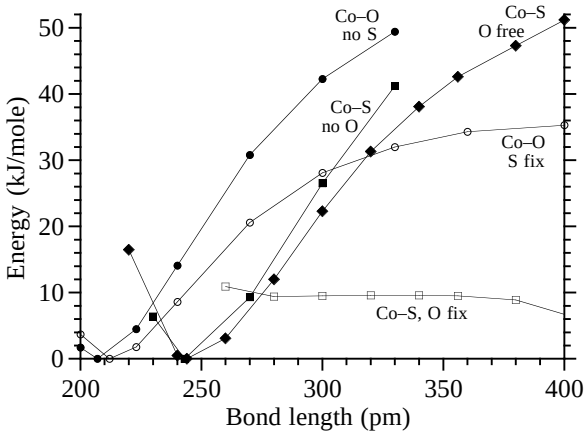

Figure 3. Potential surfaces for the Co–O and Co–S_{Met} bonds in three models of Co(II)-substituted azurin [37]. "No S" and "no O" refer to the Co(Im)($ImCH_2CH_2NHCOCH_3$)-$(SCH_3)^+$ and Co$(Im)_2(SCH_3)(S(CH_3)_2)^+$ models, respectively, whereas the other two curves were obtained with the Co(Im)($ImCH_2CH_2NHCOCH_3$)$(SCH_3)(S(CH_3)_2)^+$ model with the Co–O or Co–S_{Met} bonds either at their equilibrium distance or fixed at the crystal values, 223 or 356 pm, respectively.

$Cu^{II}(NH_3)_3X$, where X is OH^-, SH^-, SeH^-, Cl^-, NH_2^-, and some other ligands related to the cysteine thiolate group [65]. The results show that all complexes may assume two types of structures, both reflecting the Jahn–Teller instability of the tetrahedral Cu(II) complex (a d^9 ion). This instability can be lifted either by a D_{2d} distortion, leading to a tetragonal structure, or by a C_{2v} distortion, leading to a trigonal structure. The tetragonal structure is stabilised by four favourable σ interactions between the singly occupied Cu 3*d* orbital and p_σ orbitals on the four ligands, as is shown in Figure 4. This gives rise to the well-known square-planar Cu(II) complexes.

If one of the ligands instead has the ability to form a strong π bond with the copper ion, however, a trigonal structure can be stabilised. The right-hand side of Figure 4 shows that in such a structure, two of the ligands still form σ bonds to the copper ion, whereas a p_π orbital of the third ligand overlaps with two lobes of the singly occupied Cu 3*d* orbital. Thereby it occupies two positions in a square coordination plane, giving rise to a trigonal planar geometry. The fourth ligand cannot overlap with the singly occupied orbital and has to interact with a doubly occupied orbital. Since such an interaction is weaker, it becomes an axial ligand with an enlarged copper distance. Thus, the long axial bond is a result of the electronic structure. Moreover, the effective coordination number is decreased, so the three strong ligands in the trigonal complex bind at shorter distances to the copper ion than in the tetragonal complex. This explains the short Cu–S_{Cys} bond in the blue copper proteins, together with the fact that a π bond to copper is inherently shorter than a corresponding σ bond [34,39].

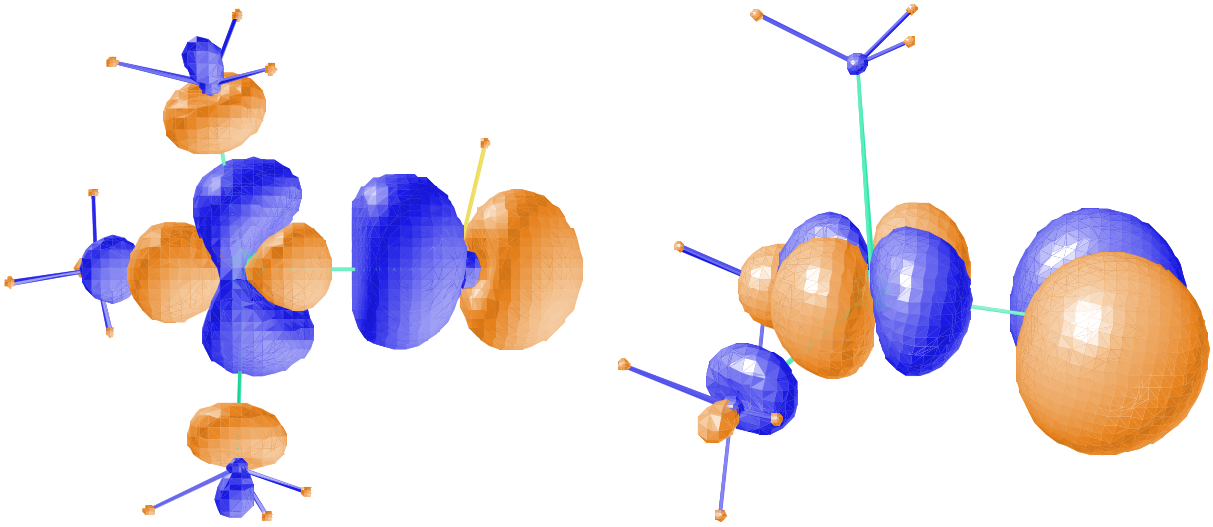

Figure 4. The singly occupied orbitals of the tetragonal (left) and trigonal (right) $Cu(NH_3)_3(SH)^+$ complex [38].

For small and hard *X* ligands, such as NH_3 and OH^-, the tetragonal $Cu^{II}(NH_3)_3X$ structure is most stable (by 30–70 kJ/mole) [65]. For large, soft, and polarisable ligands, such as SH^- and SeH^-, on the other hand, the two types of structures have approximately the same stability (within 15 kJ/mole). Interestingly, the tetragonal structure is most stable for $Cu(NH_3)_3(SH)^+$, whereas the trigonal structure is more stable for $Cu(NH_3)_2(SH)(SH_2)^+$, showing that the methionine ligand is also important for the structure of the blue copper proteins. This explains why very few trigonal cupric structures have been observed for small inorganic models; there simply is no complex with the appropriate set of ligands, $CuN_2S^-S^0$ [63,66,67].

Formally, the $Cu(NH_3)_3X$ complexes consist of a Cu(II) ion with nine *d* electrons and a neutral or negatively charged *X* ligand. For three soft and negatively charged ligands, SeH^-, NH_2^-, and PH_2^-, however, the charge on the ligand moves to copper ion, yielding a Cu(I) ion and an uncharged ligand radical. Since the Cu(I) ion has a full *d* shell, it prefers a tetrahedral structure and the complexes with these three ligands are almost tetrahedral. The thiolate ligand is intermediate: the electron is delocalised between the copper and thiolate ions. Therefore, both the trigonal and the tetragonal structures are rather tetrahedral and are actually quite similar (c.f. Figure 4). Naturally, this facilitates electron transfer to and from the complex by reducing the reorganisation energy.

A characteristic difference between the two geometries of $Cu(NH_3)_2(SH)(SH_2)^+$ is that the tetragonal structure has a longer $Cu–S_{Cys}$ bond and a shorter $Cu–S_{Met}$ bond than the trigonal structure. Moreover, the φ angle (the angle between the S–Cu–S and N–Cu–N planes) is smaller in the tetragonal structure and the two largest angles around the copper ion in the trigonal structure are between S_{Cys} and the two N_{His} atoms, whereas in the tetragonal structure the two largest angles are between two distinct pairs of atoms (S_{Cys}–Cu–N and S_{Met}–Cu–N).

These structural differences remind of the differences in the crystal structure of plastocyanin and nitrite reductase (c.f. Table 1). Detailed investigations have shown that this is not accidental: Plastocyanin, and more generally, axial type 1 copper proteins have a trigonal structure with a π bond between copper and the thiolate ligand, whereas the so-called rhombic type 1 copper proteins (e.g. nitrite reductase) have a tetragonal structure with mainly σ bonds to the copper ion (c.f. Figures 6 and 7). This gives an attractive explanation to the structural and spectroscopic differences between these proteins, which share the same copper ligand sphere [34,65]. The two types of structures have almost the same energy (within 7 kJ/mole) and which structure is most stable depends on the models used for the ligands. At present it is not possible to decide if the native structure of the typical blue-copper ligand sphere is trigonal or tetragonal [26,34,54,65].

Thus, with the typical blue-copper ligands, the tetragonal Jahn–Teller distortion may at worst give rise to the structure found in nitrite reductase, i.e. a fully functional site with properties (reduction potentials and reorganisation energies) similar to those of the trigonal blue copper proteins [35,68]. This shows that with the blue-copper ligands there is no need for protein strain to avoid a tetragonal structure.

By free energy perturbations, we have studied why some proteins stabilise the trigonal structure, whereas others stabilise the tetragonal structure, although the ligand sphere is the same [54]. The results indicate that plastocyanin prefers the bond lengths and electrostatics of the trigonal structure, whereas nitrite reductase favours the angles in the tetragonal structure, both by 10–20 kJ/mole. Interestingly, the length of the Cu–S_{Met} bond has a very small influence on the relative stability of the two conformations.

The existence of trigonal and tetragonal structures seems to be general for copper–cysteine complexes. An illustrative example is the geometry of the catalytic metal ion in copper-substituted alcohol dehydrogenase (the native enzyme contains zinc). In this enzyme, the copper ion is coordinated by two cysteines, one histidine, and a ligand from the solution. A crystal structure with dimethylsulfoxide as the fourth ligand shows a trigonal structure with dimethylsulfoxide as an axial ligand at a large distance (319–345 pm) [69]. Our calculations [39] show that the electronic structure of such complexes is very similar to the traditional blue copper proteins. The N_{His} atom and one of the S_{Cys} atoms make σ bonds to the copper ion, whereas the other S_{Cys} atom forms a π bond with copper. Thus, the two cysteine ligands are not equivalent; the π bonded ligand has a shorter Cu–S_{Cys} bond and larger angles to the other ligands compared to the σ bonded ligand (217 and 225 pm, respectively).

Tetragonal structures may also be obtained for models of Cu–alcohol dehydrogenase [39]. When the fourth ligand is uncharged, they are less stable than the corresponding trigonal complexes (in accordance with the crystal structure). However, with OH^- (which is involved in the reaction mechanism of the enzyme)

Table 2. The effect of the model size, basis set, and density functional method on the geometry of the trigonal models of the oxidised blue-copper site [26].

Method	Model[a]	Basis	Distance to Cu (pm)			Angle around Cu (°)				φ
		set[b]	S_{Cys}	N	S_{Met}	N–N	S_{Cys}–N	S–S	S_{Met}–N	(°)
B3LYP	1	1	218	204-205	267	103	119-122	117	94-95	89.1
B3LYP	1	2	219	206	269	104	119-122	117	94-96	88.5
B3LYP	1	3	218	205	267	103	118-123	117	94-96	88.3
B3LYP	2	1	218	204-206	271	102	120-125	115	94-95	89.7
BP86	1	1	219	203-210	236	103	102-130	116	99-105	81.1

[a] The models are 1, $Cu(Im)_2(SCH_3)(S(CH_3)_2)^+$ or 2, $Cu(ImCH_3)_2(SC_2H_5)(S(CH_3)(C_2H_5)^+$.
[b] The basis sets are 1, DZpdf/6–31G*; 2, TZVPP; or 3, DZs2pd2f /6-311(+)G(2d,2p) [26].

as the fourth ligand, the tetragonal structure is most stable. This may explain some of the spectral shifts that are observed experimentally when the coenzyme or the ligands are exchanged [69].

2.3 The sensitivity of the geometries to the theoretical method

When we did the geometry optimisations of the plastocyanin models six years ago, they were on the verge of the possible; each optimisation took three CPU-months. Today, such calculations can be done routinely in less than a week on a standard workstation. Therefore, we now have the opportunity to test whether these calculations were converged with respect to the basis sets or model systems. In Table 2, we list the result of a series of such calculations for the oxidised trigonal plastocyanin model, $Cu(Im)_2(SCH_3)(S(CH_3)_2)^+$ [26]. Clearly, the results are very stable. If the basis set is enhanced to triple-ζ, with diffuse functions on S and N, and double polarising functions on all atoms (DZs2pd2f/6–311(+)G(2d, 2p) [25]) or is changed to the TZVPP basis set (with a *d* function on H and an *f* function on other atoms) [70], the bond lengths to copper change by less than 2 pm and the angles change by less than 1°. Similarly, if a methyl group is added to all ligands ($Cu(ImCH_3)_2(SC_2H_5)(C_2H_5SCH_3)^+$), only small changes are observed, up to 4 pm in the bond length and 3° in the angles.

It would have been interesting to check if the results also are converged with respect to the method. Unfortunately, there is no method that is clearly better and can be used for models of this size. It is still not possible to do analytical geometry optimisations with the CASPT2 method and test calculations with the MP2 method indicate that these results cannot be converged with respect to the basis set [26]. Therefore, we have only made calculations with another common density functional method, Becke–Perdew86 (BP86) [71,72]. In general performance, it slightly less accurate than B3LYP [22], but it has the advantage of lacking exact exchange, which may in combination with other techniques make the calculations about five times faster than B3LYP [73]. However, as can be seen in Table 2, the change in the density functional, leads to quite appreciable changes in the geometry, up to 10° in the angles and as much as 35 pm for the Cu–S_{Met}

Table 3. The effect of the dielectric constant (ε) on the geometry of the $Cu(Im)_2(SCH_3)$-$(S(CH_3)_2)$ complex [26]. The calculations were performed with the B3LYP method, the DZpdf/6–31G* basis set, and the CPCM solvation model with a water probe.

ε	Distance to Cu (pm)				Angle around Cu (°)			φ
	S_{Cys}	N	S_{Met}	N–N	S_{Cys}–N	S–S	S_{Met}–N	(°)
1	232	214–215	237	109	105–108	115	107–113	89.4
2	233	209–211	240	116	106–108	106	103–115	87.0
4	234	209–211	241	117	107–109	105	103–114	86.8
8	233	209–210	244	118	108–112	106	100–112	86.7
16	235	208–208	246	120	108–110	104	103–110	87.6
80	232	208–211	248	112	108–121	104	98–110	87.4

bond length. Even if these changes are not so large in energy terms, the structure is appreciably less similar to the experimental structures and therefore we cannot recommend this method for general use.

Similar results apply for the reduced models, but due to the weaker interaction with copper, the changes are slightly larger, up to 6 pm and 7° [26]. Most importantly, however, the relative energy between the optimal geometry and the complex with the Cu–S_{Met} bond length fixed at 290 pm is converged; it changes by less than 1 kJ/mole if the basis set or model system is increased. With the Becke–Perdew86 method, bond lengths change by up to 9 pm, angles by less than 4°, but the relative energy change by 6 kJ/mole [26].

Our study of the reduction potential of the blue copper proteins indicated that the geometries may change quite appreciably when solvation effects are taken into account [35]. We have therefore performed a number of geometry optimisations of the reduced $Cu(Im)_2(SCH_3)(S(CH_3)_2)$ complex in a solvent with varying values of the dielectric constant [26]. The results in Table 3 show that the bond lengths change by up to 11 pm and the angles by up to 11°. Thus, the geometry change in the solvent, but the effects are not very large, and the general geometry is not changed (the φ angle does not decrease below 86°). In particular, the effect of the solvent is smaller than the results for the reduction potential indicate.

It is notable that the length of the Cu–S_{Met} bond increases with the dielectric constant. Thus, solvent effects may explain parts of the difference between the optimised and crystal structures for the reduced complexes. Even if the Cu–S_{Met} bond does not become longer than 248 pm, this will decrease the energy difference between the optimised and the crystal structure (i.e. below 4 kJ/mole). Furthermore, increasing the basis set [26], the model size [26], or improving the theoretical method [14] also elongate the Cu–S_{Met} bond, as do dynamic effects [54]. If all these corrections are added together, the Cu–S_{Met} bond length should become ~270 pm, but non-additive effects may make it even longer. Therefore, it is not clear if there is any discrepancy at all between the calculated and experimental length of this bond, but if there is any, it is very small in energy terms.

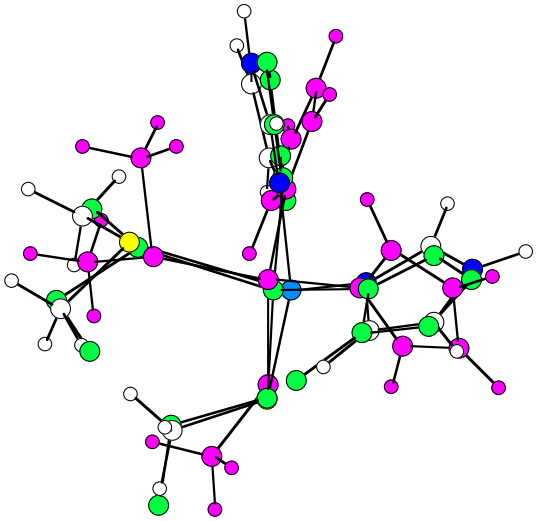

Figure 5. A comparison between the crystal structure of reduced plastocyanin (light grey and no hydrogen atoms) [74] and the structures of $Cu(Im)_2(SCH_3)(S(CH_3)_2)$ optimised in vacuum (dark grey) [14] or with COMQUM in reduced plastocyanin [26].

2.4 Geometry optimisations in the protein

The best way to study the geometry of the blue copper proteins is to perform geometry optimisations in the protein using combined quantum chemical and molecular mechanical methods. We have recently initiated a series of such calculations using the program COMQUM [57], which uses the B3LYP method for the active site and the Amber force field [40] for the rest of the protein [26]. Some of the results of these calculations are shown in Table 4.

It is clear that the COMQUM structures are appreciably more similar to crystal structures than structures optimised in vacuum. This is most obvious for the orientation of the histidine rings and the dihedrals of the other copper ligands, as can be seen in Figure 5. This improvement is quite natural since these low-energy modes are determined in vacuum by weak hydrogen bonds involving the methyl groups. In the protein, they are instead determined by interactions with the surrounding protein, e.g. steric effects, normal hydrogen bonds, and non-polar interactions.

However, there is also a significant improvement of the Cu–ligand distances and the angles around the copper ion, as can be seen in Table 4. In all COMQUM structures, the $Cu–S_{Cys}$ bond is appreciably shorter than in vacuum, which make them more similar to what is found in crystal structures (they still are a few pm too long, which reflect the tendency of B3LYP to give too long $Cu–S_{Cys}$ bonds [14]). This is probably an effect of the $NH^{\cdots}S_{Cys}$ hydrogen bond in the protein. Similarly, the Cu–N distances are 3–10 pm shorter than in the vacuum structures, again improving the agreement with crystal structures. The $S–Cu–S_{Met}$, $S_{Met}–Cu–N$, and φ angles are also significantly improved, especially for the oxidised systems.

Table 4. The result of COMQUM calculations on plastocyanin, nitrite reductase, and cucumber basic protein, using the quantum system $Cu(Im)_2(SCH_3)(S(CH_3)_2)^+$ [26].

	System[a]		Distance to Cu (pm)			Angle around Cu (°)				φ
Cu	Protein	Con	S_{Cys}	N	S_{Met}	N–N	S_{Cys}–N	S–S	S_{Met}–N	(°)
I	Vacuum		232	214–215	237	109	105–108	115	107–113	89
	Pc red	Yes	221	203–208	339	103	120–134	104	78–101	76
		No	222	203–212	375	103	120–136	105	72–103	71
	Crystal		211–217	203–239	287–291	91–118	110–141	99–114	83–110	74–80
II	Vacuum		218	204	267	103	120–122	116	94–95	90
	Pc ox	Yes	214	197–198	290	103	123–125	105	86–106	78
	Crystal		207–221	189–222	278–291	96–104	112–144	102–110	85–108	77–89
II[b]	Vacuum		223	205–206	242	100	97–141	103	95–126	62
	Nir	Yes	219	200–203	262	100	104–135	105	87–129	61
		No	224	203–205	241	97	91–146	105	89–141	48
	Crystal		208–223	193–222	246–270	96–102	98–140	103–109	84–138	56–65
II[c]	CBP	Yes	217	199–210	273	100	118–128	104	84–118	69
	Crystal		216	193–195	261	99	110–138	111	83–112	70

[a] The system is defined by the oxidation state of the copper ion (Cu), the protein (Pc red, reduced plastocyanin; Pc ox, oxidised plastocyanin; CBP, cucumber basic protein; Nir, nitrite reductase; Vacuum, quantum chemical optimisation in vacuum [14,34]; Crystal, range observed in the available crystal structures in the Brookhaven protein data bank), and whether there is a connection between the metal ligands and the protein backbone (Con).

[b] This is the tetragonal structure, which in vacuum is obtained with the $Cu(Im)_2(SH)(S(CH_3)_2)^+$ model [34,65].

[c] This is a structure intermediate between trigonal and tetragonal that has not been observed in vacuum.

For the Cu–S_{Met} bond length, the results are less clear. In all cases, the bond is elongated, and for the oxidised structures, it is in excellent agreement with experimental structures. However, for reduced plastocyanin, the Cu–S_{Met} bond becomes too long, 339 pm, compared to ~290 pm. This is most likely due to the flexibility of the bond, combined with problems in the classical force field. Apparently, the molecular mechanics part of the calculations is not accurate enough to describe the fine-tuned interplay between methionine group, the copper ion, and the surrounding enzyme.

Nitrite reductase and cucumber basic protein were also included in the investigation to see if the protein could stabilise tetragonal and intermediate structures, although such structures cannot be found in vacuum with the quantum system used ($Cu(Im)_2(SCH_3)(S(CH_3)_2)^+$). The results in Table 4 show that this is actually the case. The COMQUM structures give φ angles of 61° and 69°, respectively, which is close to the experimental values and clearly show that the nitrite reductase is tetragonal, whereas the cucumber basic protein structure is intermediate. The large S_{Met}–Cu–N and S_{Cys}–Cu–N angles also flag that the structures are not trigonal.

At first, these improved structures could be taken as evidence for protein strain. However, the COMQUM calculations involve effects that are normally not considered as strain, e.g. the change in the dielectric surrounding of the copper

site, electrostatic interactions, and hydrogen bonds. In order to distinguish between these effects, we performed two calculations in which the covalent bond between the backbone and the side chain of the metal ligands is removed (c.f. Table 4) [26]. This way, covalent strain effects from the protein are eliminated. Interestingly, this hardly changed the structure of the plastocyanin site at all, except for an elongated Cu–S_{Met} bond. However, the nitrite reductase structure became more similar to the vacuum structure, except for a larger variation in the S_{Met}–Cu–N angles and a smaller φ angle (even smaller than in crystal structures). Thus, the nitrite reductase structure seems to be tuned by covalent interactions, whereas the plastocyanin site is modified by electrostatic interactions. This is in excellent agreement with our free energy calculations of the two proteins [54], which indicated that plastocyanin preferred the trigonal structure by electrostatic interactions, whereas nitrite reductase favoured the angles in the tetragonal structure. It should be noted, however, that already the vacuum structures reproduce most of the features of the copper coordination. Protein interactions are used only to fine-tune the structures at a small cost in energy.

Actually, the COMQUM calculations give us an opportunity to directly estimate strain energies in the proteins. The strain energy is given by the difference in energy of the isolated quantum system at the COMQUM geometry and at the optimal vacuum geometry. This energy ranges from 33 to 51 kJ/mole. This is similar to what was found for the catalytic and structural zinc ions in alcohol dehydrogenase, 30–60 kJ/mole [57,75–77], which seems to be a normal strain energy for the incorporation of a metal site from vacuum into a protein.

If the connection between the protein and the metal ligands is removed, the strain energy is approximately halved. The difference (21–23 kJ/mole) is close to the strain energy in the sense of Warshel [50] (see Section 8) and also in the common mechanical sense (a distortion of the structure caused by covalent interactions). This energy is actually appreciably *lower* than what was found for alcohol dehydrogenase (33 kJ/mole) [76]. Yet, even these energies involve some terms that are not commonly regarded as strain. In the vacuum structure there are hydrogen bonds between the methyl groups and the negatively charged S_{Cys} atom. These are removed in the COMQUM structure, but the more favourable interactions in the protein are not included when the strain energies are calculated. This gives a significant positive contribution to the strain energy. Therefore, it is not surprising that the strain energies are still not negligible, but it is clear that the COMQUM calculations give no evidence of any unusual strain energies for the blue copper proteins.

4. ELECTRONIC SPECTRA

The hallmark of cupredoxins, leading to their description as blue or type 1 copper proteins, is the presence in their electronic spectrum of an intense (ε = 3 000–6 000 $M^{-1}cm^{-1}$) absorption band around 600 nm. This spectral feature distinguishes them from normal inorganic Cu(II) complexes, the spectrum of which only contains a number of weaker (ε = 100 $M^{-1}cm^{-1}$) ligand-field transitions in the same region [78]. However, also within the type 1 proteins, variations exist. In addition to the prominent peak at 600 nm, a feature at 450 nm is observed in all spectra with a varying intensity [79,80]. The axial type 1 proteins, like plastocyanin and azurin, show only little absorption in the 450-nm region, whereas this band becomes much more prominent in rhombic type 1 proteins, like pseudoazurin, cucumber basic protein, and stellacyanin. The increasing intensity of the 450–nm band in the latter proteins goes together with a decrease in intensity of the 600–nm band, so the sum of ε_{460} and ε_{600} is approximately constant [79]. Nitrite reductase from *Achromobacter cycloclastes* is a limiting case for which the 460-nm line is actually more intense than the 600-nm peak, giving the enzyme a green colour. No natural proteins exist in which the blue band is even further reduced, but by site-directed mutagenesis a number of mutants have been constructed in which only the second band is present, blue-shifted towards 410 nm, giving them a yellow to orange colour [81]. Based on the analogy of their EPR spectra with the normal type 2 copper proteins, these mutants have been classified as type 2 [82]. The classification of mutants with intermediate spectroscopic characteristics as type 1.5 follows naturally.

Apart from these two peaks, several weaker features have been discerned in the visual and near-infrared region of the spectra of type 1 copper proteins. Based on different types of spectroscopic analyses and with the help of the density functional Xα calculations, Solomon and coworkers [83,84] have reported and assigned a total of nine absorption bands in the spectrum of plastocyanin (c.f. Table 5). They assigned the 600-nm (11 700 cm^{-1}) band to a charge transfer excitation from a S_{Cys} *p* orbital with π overlap to a Cu orbital. The band at 460 nm (21 370 cm^{-1}) was proposed to correspond to a His→Cu charge-transfer, whereas an additional feature at 535 nm (18 700 cm^{-1}) was assigned to a charge transfer from the so-called S_{Cys} pseudo-σ orbital. Similar studies have more recently been performed on nitrite reductase [85], cucumber basic protein, and stellacyanin [86]. Below, we describe our spectroscopic studies of the blue copper proteins with the more accurate CASPT2 method, leading to a unified theory for the spectra of copper–cysteinate proteins.

4.1 The electronic spectrum of plastocyanin

We have studied the electronic spectrum of plastocyanin with the CASSCF/CASPT2 approach [36]. The blue copper site in this protein is not symmetric. However, the N–Cu–N and S–Cu–S planes are approximately perpendicular, so the geometry can be changed to C_s symmetry with modest movements. Such a symmetrisation simplifies the labelling of the excited states and speeds up the calculations, so that larger models and more excited states can be studied. However, our most reliable results were obtained for an unsymmetrical $Cu(Im)_2(SH)(SH_2)^+$ model (for which we can include a point-charge model of the surrounding protein and solvent), corrected for the truncated cysteine and methionine models [36]. A total of nine states have been studied, including the five ligand-field states and the four lowest ligand-to-metal charge-transfer states. The results are shown in Table 5 together with experimental excitation energies.

The various excited states can best be characterised by analysing the singly occupied molecular orbital of each state. These orbitals are shown in Figure 6. The singly occupied orbital for the X ^{2}A" ground state is strongly delocalised over the Cu–S_{Cys} bond. It involves a π antibonding interaction between the Cu $3d_{xy}$ and S_{Cys} $3p_y$ orbitals, combined with a much weaker σ antibonding interaction with the two N ligands, whose positions in the equatorial plane are such that a perfect σ overlap with the two remaining lobes of the Cu $3d_{xy}$ orbital is obtained (the coordinate system is selected so that the copper ion is in the origin, S_{Met} is on the z axis, and S_{Cys} is in the xz plane).

The singly occupied orbital of the first excited state (a ^{2}A') is formed by a σ antibonding combination of the Cu $3d_{x^2-y^2}$ and S_{Cys} $3p_x$ orbitals. This interaction is also strongly covalent. The calculated excitation energy for this state is 4 119 cm^{-1}, which explains the appearance of the band at 5 000 cm^{-1} in the plastocyanin spectrum. Between 10 000 and 14 000 cm^{-1}, three bands are found in the experimental spectrum, corresponding to the calculated states b ^{2}A', b ^{2}A", and c ^{2}A'. From the composition of the corresponding singly occupied orbitals it is clear that the states concerned can be labelled as genuine ligand-field states, with the electron hole localised in the Cu $3d_{z^2}$, $3d_{yz}$, and $3d_{xz}$ orbitals, respectively. The presence of a definite amount of S_{Cys} $3p_\pi$ character in the Cu $3d_{yz}$ orbital of the b ^{2}A" state is notable. This mixing gives a significant intensity for the transition to this state, which is in fact responsible for the second most intense band in the plastocyanin spectrum.

The dominant blue band, appearing at 16 700 cm^{-1} in the experimental spectrum, was calculated at 17 571 cm^{-1} and corresponds to the c ^{2}A" state. As can be seen from Figure 6, the corresponding singly occupied orbital is the bonding counterpart to the Cu–S_{Cys} π antibonding ground-state orbital. The extremely good overlap between the two orbitals immediately explains the large absorption intensity of the corresponding excitation. Even if this transition formally can be

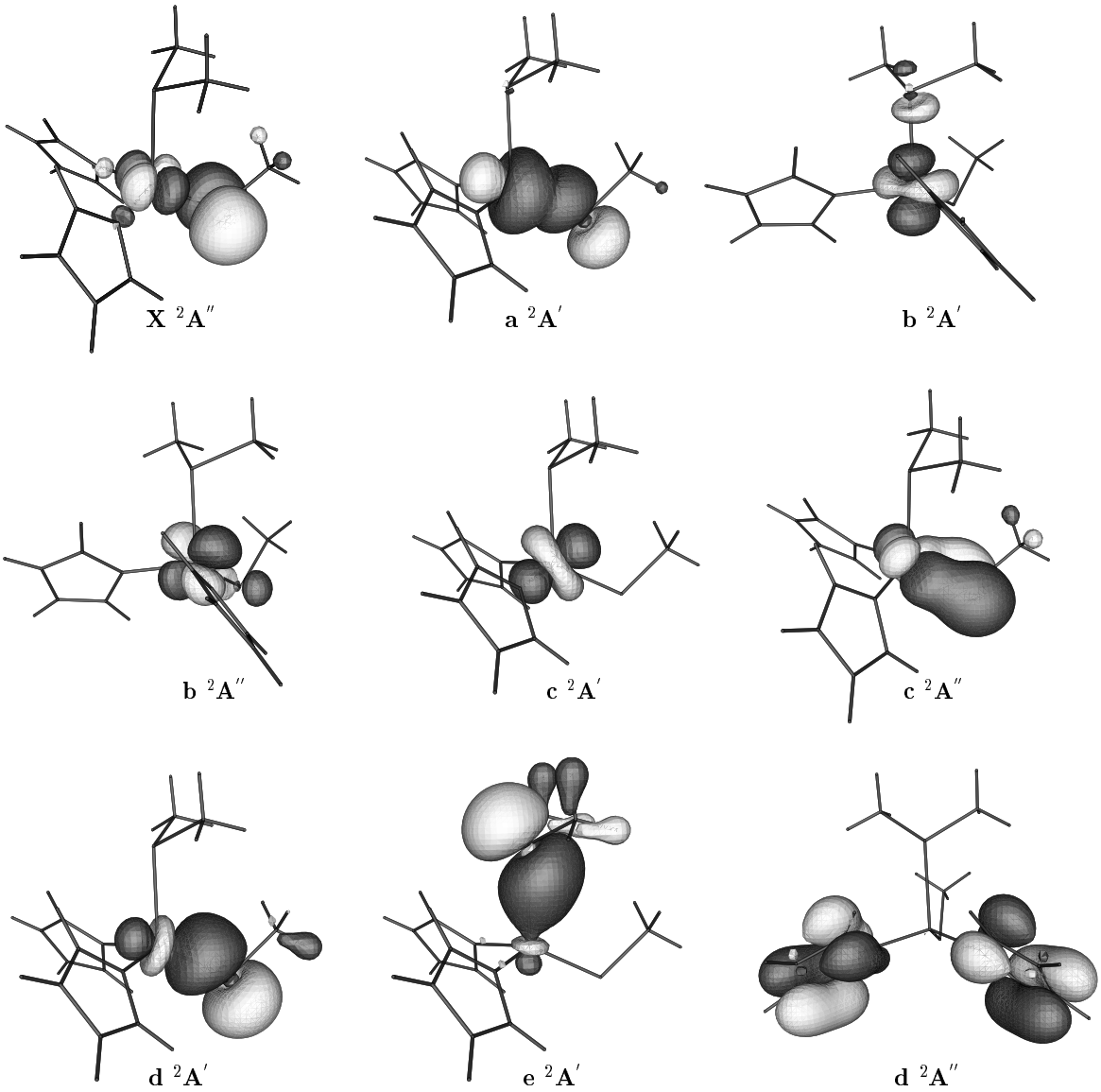

Figure 6. The singly occupied orbitals of the various excited states in the symmetric $Cu(Im)_2$-$(SCH_3)(S(CH_3)_2)^+$ model, calculated at the CASSCF level [36].

labelled as a $S_{Cys} \rightarrow Cu$ charge-transfer excitation, the actual amount of charge transferred is only about 0.2 *e*.

At higher energies, four additional charge-transfer bands were observed in the experimental spectrum, at 18 700, 21 390, 23 440, and 32 500 cm^{-1}, respectively [84]. The latter two bands were assigned by Gewirth and Solomon [84] as charge-transfer excitations from methionine and histidine, respectively. We could only study these excitations in models with enforced symmetry. The results are therefore more approximate than for the lower excitations, but they are in line with Gewirth's assignments.

However, for the bands at 18 700 and 21 390 cm^{-1}, there is a discrepancy between the experimental spectrum and our calculations. Indeed, we predict only

Table 5. The experimental [84,85] and calculated [34,36] spectrum of plastocyanin and nitrite reductase (excitation energies in cm^{-1}, oscillator strengths in brackets) together with the assignment of the various excitations. The ground-state singly occupied orbital is Cu–S_{Cys} π* in plastocyanin but Cu–S_{Cys} σ* for nitrite reductase.

State	Plastocyanin			Nitrite reductase		
	Assignment	Calculated	Experimental	Experimental	Calculated	Assignment
a ^{2}A'	Cu–S_{Cys} σ*	4 119 (0.000)	5 000 (0.000)	5 600 (0.000)	4 408 (0.000)	Cu–S_{Cys} π*
b ^{2}A'	$3d_{z^2}$	10 974 (0.000)	10 800 (0.003)	11 900 (0.003)	12 329 (0.000)	$3d_{z^2}$
b ^{2}A''	$3d_{yz}$	13 117 (0.001)	12 800 (0.011)	13 500 (0.009)	12 872 (0.000)	$3d_{yz}$
c ^{2}A'	$3d_{xz}$	13 493 (0.000)	13 950 (0.004)	14 900 (0.010)	13 873 (0.003)	$3d_{xz}$
c ^{2}A''	Cu–S_{Cys} π	17 571 (0.103)	16 700 (0.050)	17 550 (0.020)	15 789 (0.032)	Cu–S_{Cys} π
d ^{2}A'	Cu–S_{Cys} σ	20 599 (0.001)	21 390 (0.005)	21 900 (0.030)	22 461 (0.119)	Cu–S_{Cys} σ

one excited state in this region of the spectrum, d ^{2}A'. The singly occupied orbital in this state is the σ bonding combination of Cu $3d_{x^2-y^2}$ and S $3p_x$, corresponding to the antibonding orbital of the first excited a ^{2}A' state. This is Gewirth and Solomon's pseudo-σ orbital [84]. They assign the band at 18 700 cm^{-1} in the experimental spectrum as the excitation to the d ^{2}A' state and the band at 21 390 cm^{-1} as another His→Cu charge-transfer excitation. Our calculated excitation energy for the d ^{2}A' state is 20 599 cm^{-1}, between the experimental bands at 18 700 and 21 390 cm^{-1}, but closer to the latter. Still, our assignment of the 21 390-cm^{-1} band as the transition to d ^{2}A' comes mainly from an analysis of the S_{Cys} p_σ→Cu transition in other proteins and as a function of the φ angle (see the next section). According to this analysis, the transition energy should remain constant for the various proteins. Therefore, it seems unlikely that the d ^{2}A' state would appear more than 3 000 cm^{-1} lower in energy in plastocyanin (18 700 cm^{-1}) than in nitrite reductase (21 900 cm^{-1} [85]). Moreover, the intensity of the S_{Cys} p_σ→Cu transition should increase significantly with a decreasing φ angle, which is in accordance with the increasing intensity of the 460-nm peak (21 700 cm^{-1}) in the experimental spectra of the rhombic type 1 proteins. In addition, experimental evidence indicate that S_{Cys}, rather than imidazole, is involved in this band [79,87]. Therefore, it is more plausible to assign the d ^{2}A' state to the band at 21 390 cm^{-1}, although this means that we have to leave the 18 700-cm^{-1} band unassigned. It is notable that the latter band is not present in the experimental spectrum of nitrite reductase [85].

4.2 Correlation between structure and spectroscopy of copper proteins

On the basis of the electronic, resonance Raman, and EPR spectra, the cysteine-containing copper proteins have been divided into four groups: axial type 1 (e.g. plastocyanin), rhombic type 1 (e.g. nitrite reductase and stellacyanin), type 1.5, and type 2 (mutant) copper proteins [81]. We have studied the spectra of members of each group with the CASPT2 method [33,34,36,38].

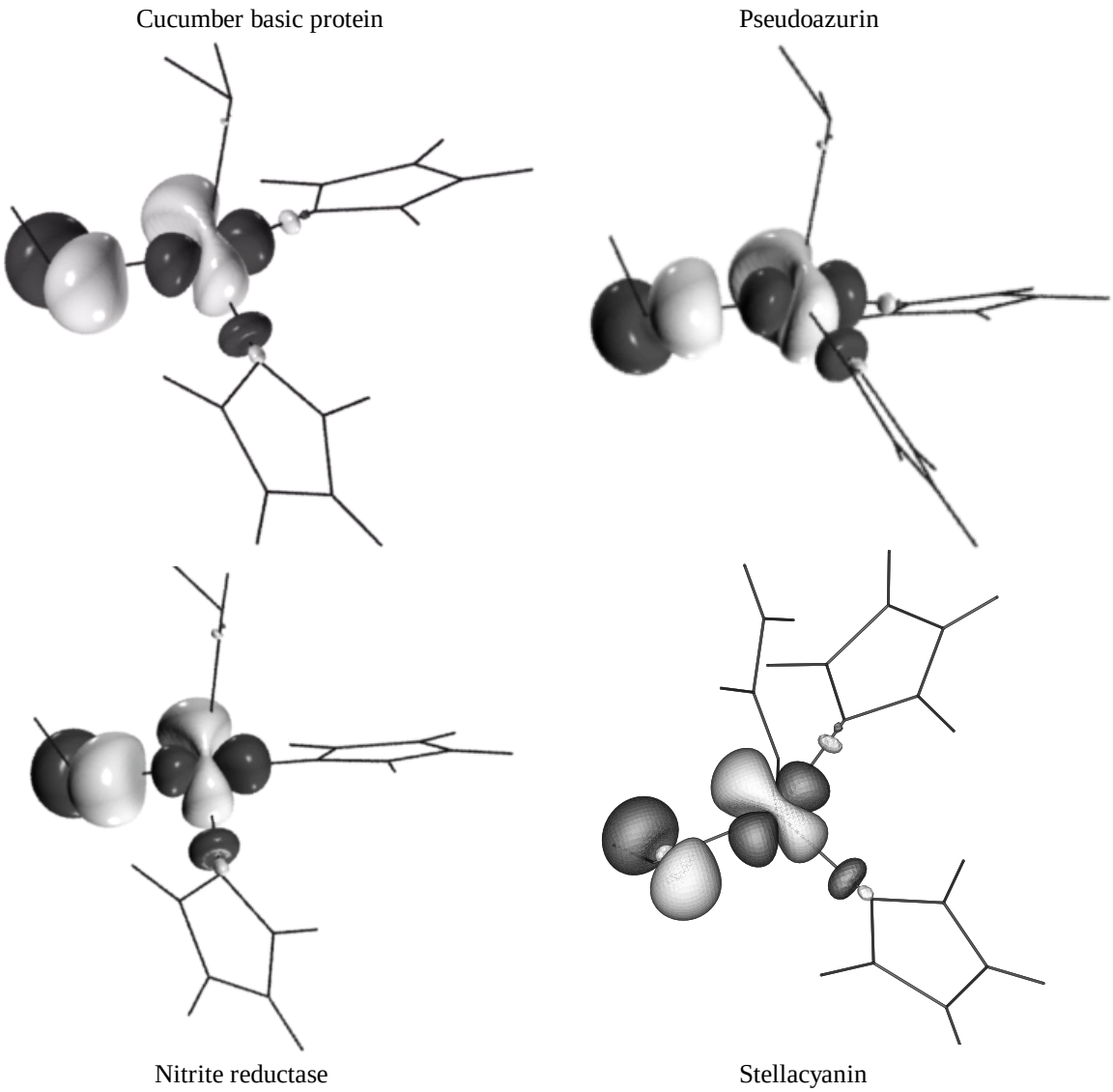

Figure 7. The singly occupied ground-state orbitals for four models of rhombic type 1 copper proteins, calculated at the CASSCF level [34].

In Figure 7, the ground-state singly occupied orbitals of three rhombic type 1 proteins, viz. cucumber basic protein (plantacyanin), pseudoazurin, and nitrite reductase, are shown. If these are compared with the ground-state orbital of plastocyanin in Figure 6, a clear difference can be seen. In plastocyanin, there is an almost pure π^* interaction between Cu and S_{Cys}. However, in nitrite reductase, this interaction is instead mainly of σ^* character, and the other two proteins show a mixture of σ^* and π^* interactions. Thus, there has been a change in the ground state of the system; for plastocyanin the Cu–S_{Cys} σ^* interaction is found in the first excited state, whereas in the rhombic proteins, a significant contribution of σ character is found in the ground-state singly occupied orbital. The singly occupied orbitals in the other excited states are not much changed. This directly explains the change in intensity pattern of the spectrum. The π^* antibonding orbital has a strong overlap with the corresponding π bonding orbital in the $c\,^2A''$ state,

giving rise to the blue line in the spectrum, whereas the σ* antibonding orbital instead overlaps strongly with the corresponding σ bonding orbital, found in the $d\,^2A'$ state. As expected, this transition gives rise to the yellow band around 460 nm in the spectrum, the line that increase in intensity for the rhombic type 1 copper proteins.

In Table 5, the calculated and experimental excitation energies and oscillator strengths of plastocyanin and nitrite reductase are compared [34]. It can be seen that the error in the calculations is consistently below 1 800 cm^{-1}, i.e. within the error limits of the CASPT2 method [28]. Moreover, the calculations follow the experimental trend, i.e. that all excitations for nitrite reductase appear at a higher energy than the corresponding excitations for plastocyanin [85]. This reflects the stronger ligand-field exerted in the tetragonal structure, with four instead of three strongly bound ligands. The intensity of the ligand-field states also reflects the change in ground state: the intensity of the $d\,^2A''$ state has dropped to zero, whereas the b,$c\,^2A'$ states gain intensity from the presence of a small amount of S_{Cys} $3p_\sigma$ character in the corresponding singly occupied orbitals.

The ground-state orbitals and the spectra of the other two proteins, cucumber basic protein and pseudoazurin are intermediate between those of plastocyanin and nitrite reductase. Similarly, their structures, as described by the angle φ between the S–Cu–S and N–Cu–N planes, are also intermediate (φ is 82, 74, 70, and 61° for plastocyanin, pseudoazurin, cucumber basic protein, and nitrite reductase, respectively). Thus, there seems to be a correlation between the spectrum and the flattening of the copper geometry. This was investigated thoroughly for the $Cu(NH_3)_2(SH)(SH_2)^+$ model by calculating the spectrum at a number of φ angles, ranging from the ideal trigonal structure (φ = 90°) to a strictly square-planar structure (φ = 0°) [34]. The results are summarised in Figure 8, which shows how the Cu–S_{Met} bond is shortened and the Cu–S_{Met} bond is elongated as the structure goes from trigonal to square planar. At the same time, the ratio of the calculated oscillator strengths for the excitations around 460 and 600 nm goes from zero to infinity. This reflects that in the trigonal structure, the $c\,^2A''$ state gives rise to the dominant blue band, whereas the $d\,^2A'$ state has little intensity. In the square-planar structure, the situation is reversed. The ground state is of Cu–S_{Cys} σ* character, and the Cu–S_{Cys} σ→σ* excitation, has by far become the most intense, whereas the $c\,^2A''$ state has almost completely vanished.

Even if the calculations were performed on a simple model, the results presented in Figure 8 nicely reflect the structure–electronic spectroscopy relationship between the various types of copper–cysteinate proteins. The copper coordination geometry of axial type 1 proteins is close to trigonal, and their spectroscopic characteristics are reflected by the results obtained for φ > 80°. Rhombic type 1 proteins like pseudoazurin and cucumber basic protein, on the other hand, have φ angles between 70° and 80°. As can be seen from Figure 8, even at such a small

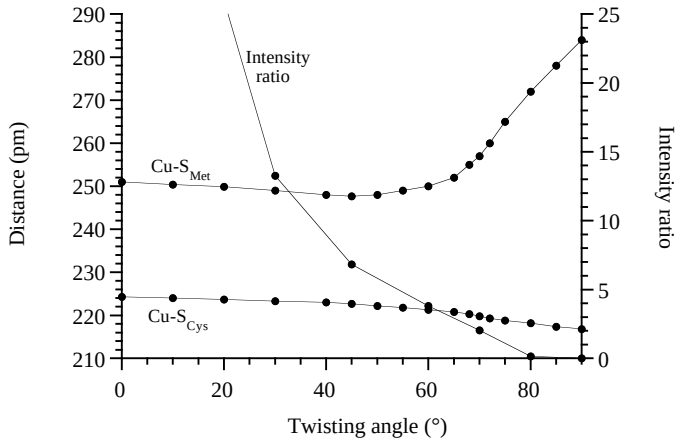

Figure 8. The variation of the Cu–S_{Cys} and Cu–S_{Met} bond lengths and the quotient of the oscillator strengths of the peaks around 460 and 600 nm as a function of the φ twisting angle [34].

deviation from orthogonality, the 460-nm excitation has already gained significant intensity due to mixing of σ character into the ground-state singly occupied orbital. The largest deviation from orthogonality within the type 1 copper proteins is found for nitrite reductase from *Achromobacter cycloclastes* which has φ = 56–65° [88]. At such angles, the second transition has become the most intense, which is in accordance with the green colour of nitrite reductase.

The intensity of the blue band further decreases as the structure is more flattened, and the results obtained for the smallest φ angles in Figure 8 can to a first approximation be used to mimic the properties of type 2 copper–cysteinate (mutant) proteins, with their yellow colour. We have also performed calculations on more realistic complexes [34,38] which confirm these predictions. They show that the Cu–S_{Cys} σ→σ* excitation is blue-shifted in these models by more than 1 000 cm^{-1}, in agreement with the experimental shift of this band from 460 to 410 nm when going from type 1 to type 2 copper proteins [81].

The result in Figure 8 has led us to suggest that axial type 1 proteins have a trigonal structure with a π bond between Cu and S_{Cys}. The other three types of copper proteins have instead a tetragonal structure with mainly σ bonds to all the four copper ligands. They differ in the flattening of the geometry, for example as described by the φ angle. Rhombic type 1 proteins, which are most distorted towards a tetrahedron, arise when one of the ligands forms a weak bond. If all ligands bind strongly, but still are rather soft (e.g. histidine), type 1.5 sites arise, whereas with harder ligands (e.g. water) and preferably with two axial ligands, the strongly flattened type 2 copper sites are found. It is notable that all sites form naturally, following the preferences of the copper ion and its ligands, and not by protein strain.

The only protein that does not fit into the above description is stellacyanin. The structure of this protein is clearly trigonal, with a φ angle of 84°, similar to plastocyanin. However, the $\varepsilon_{460}/\varepsilon_{600}$ ratio for stellacyanin is significantly higher than for plastocyanin and its ESR characteristics are rhombic instead of axial. The structure and electronic characteristics of stellacyanin were recently discussed in two independent studies by Solomon et al. and us, and quite different interpretations were given [33,86]. In Solomon's view, the stronger axial ligand in stellacyanin (a glutamine side-chain amide group, which binds closer to the copper ion than methionine, ~220 pm compared to 265–330 pm) should induce a stronger Jahn–Teller driving force. The fact that the copper surrounding in stellacyanin is not more strongly tetragonally distorted than in plastocyanin can in this view only be explained by more protein strain. However, our calculations on the $Cu(Im)_2(SCH_3)(OCCH_3NH_2)^+$ model show that its optimal geometry is trigonal and close to the crystal structure of cucumber stellacyanin (c.f. Table 1) [33]. There is no need for strain, since the Jahn–Teller instability can be lifted also by a trigonal distortion instead.

As concerns the spectral characteristics, Solomon makes a clear distinction between stellacyanin and the other rhombic type 1 proteins, in that he gives a different assignment to the intensity-gaining band around 460 nm: a His→Cu charge-transfer excitation in stellacyanin, as opposed to a S_{Cys} pseudo-σ→Cu excitation in the other rhombic proteins. As already noted, the His→Cu band was not reproduced by our calculations. However, our results indicate that the excitation out of the S_{Cys} σ orbital around 22 000 cm^{-1} becomes significantly more intense in stellacyanin, at the expense of the blue band, in conformity with what was found for the other rhombic type 1 proteins. The intensity-gaining mechanism in stellacyanin is not a decreasing φ angle, but the stronger axial interaction with the glutamine side-chain amide group, giving rise to a more pronounced mixing in of σ character into the ground-state singly occupied orbital, even in an almost strictly trigonal structure (see Figure 7d) [33]. Therefore, there is no need to invoke a His→Cu excitation to explain the increased $\varepsilon_{460}/\varepsilon_{600}$ ratio in stellacyanin.

4.3 The sensitivity of the calculated spectra on the theoretical method

Our studies of the spectra of blue copper proteins have taught us a lot about spectra calculations on metal complexes and their sensitivity to various parameters. First, the size of the ligand models is crucial. Imidazole should be used as a model of histidine, SCH_3^- for cysteine, $S(CH_3)_2$ for methionine, and CH_3CONH_2 for glutamine [33,36]. If imidazole is replaced by NH_3, most excitation energies decrease by 800–1900 cm^{-1}, and the ordering of the excitations may change. Likewise, if SCH_3^- is replaced by SH^-, the excitation energies decrease by up to 5 200 cm^{-1}. On the other hand, substituting SH_2 for $S(CH_3)_2$ *increases* all excitations by up to 6 800 cm^{-1}. Consequently, the results obtained with $Cu(Im)_2$-

$(SH)(SH_2)^+$ and $Cu(Im)_2(SCH_3)(S(CH_3)_2)^+$ are quite similar, and can be improved by a set of corrections factors [33,34,36]. Further replacing SCH_3^- with $SC_2H_5^-$ has a small effect on all excitation energies (less than 200 cm^{-1}). This is a bit surprising, since Zerner et al. report changes of up to 2 100 cm^{-1} in the spectrum of rubredoxin when the chromophore is modelled by $Fe(SC_2H_5)_4$ instead of $Fe(SCH_3)_4$ [89].

Second, the geometry strongly influences the spectrum. In particular, the Cu–S distances are crucial. If the $Cu–S_{Cys}$ distance is decreased by 5 pm, all excitation energies increase by up to 2 000 cm^{-1}. Similarly, if the $Cu–S_{Met}$ bond length is increased by 10 pm, the excitation energies increase by up 900 cm^{-1}, except for the excitation to the $e\,^2A'$ state (the charge-transfer to methionine), which change by 1 900 cm^{-1} [36]. Therefore, in order to reproduce experimental excitation energies and to get accurate results it is necessary to reoptimise the two Cu–S distances with the CASPT2 method [34].

Third, the effect of the surrounding protein and solvent molecules, which has been estimated using a point-charge model, is appreciable and cannot be neglected. The general trends are the same for all proteins studied, and can be related to the character of the transitions [33,34,36,39]. The excitation energies of the two $S_{Cys}\rightarrow Cu$ charge-transfer states increase by up to 2 800 cm^{-1}, whereas the ligand-field excitations, which involve an appreciable charge-flow from Cu to S_{Cys}, decrease by almost 2 000 cm^{-1}. A considerably smaller effect is found for the lowest transition, which is essentially a transition within the $Cu–S_{Cys}$ bond. However, if only details in the crystal structure are changed, e.g. the binding or exchange of the coenzyme (NADH) in Cu-substituted alcohol dehydrogenase, the variation in the spectra is limited, less than 300 cm^{-1} [39]. It is also notable that the surroundings reduce all oscillator strengths by a factor of up to 1.75.

Finally, we have also investigated the influence of the basis sets, relativistic effects, and Cu 3*s* and 3*p* semicore correlation on the spectrum [36]. Somewhat unexpectedly, the spectrum is quite insensitive to the basis set. Increasing it with double polarising functions on Cu and S and single polarising functions on C, N, and H, change the spectrum by less than 250 and 500 cm^{-1} for the ligand-field and charge-transfer states, respectively, except for the charge-transfer state from methionine, which is changed by 2 300 cm^{-1} [36]. Likewise, relativistic effects and the Cu 3*s* and 3*p* correlation do not influence the spectrum very much, less than 800 cm^{-1} [36]. However, the two effects act in the same direction and change the ligand-field and the charge transfer excitations in opposite directions (both effects favour states with a low Cu 3*d* population). Thus, their combined effect may significantly alter the relative energy of the excited states. Therefore, they are included in all reported excitation energies.

5. REORGANISATION ENERGIES

According to the semiclassical Marcus theory [6], the rate of electron transfer depends on the reduction potential (ΔG_0), the electronic coupling matrix element (H_{DA}), and the reorganisation energy (λ):

$$k_{ET} = \frac{2\pi}{\hbar} \frac{H_{DA}^2}{\sqrt{4\pi\lambda RT}} \exp\left(\frac{-(\Delta G_0 + \lambda)^2}{4\lambda RT}\right). \quad (1)$$

If the geometry of the active site and its surroundings does not change much during electron transfer, the reorganisation energy will be small, and the reaction will be fast. Therefore, it is of vital importance for an electron-transfer protein to reduce the reorganisation energy. For convenience, the reorganisation energy is usually divided into two parts: inner-sphere reorganisation energy, which is associated with the structural change of the first coordination sphere, and outer-sphere reorganisation energy which involves structural changes of the remaining protein as well as the solvent.

Several groups have tried to estimate the reorganisation energy for transition-metal complexes and proteins using theoretical methods of variable sophistication and with varying success [51,90–101]. However, we seem to be the only group that has systematically studied models with relevance to the blue copper proteins. We have estimated inner-sphere reorganisation energies by calculating the energy difference of a reduced model between the optimum geometry of the reduced and oxidised complex or vice versa [68]. For our best model of plastocyanin, $Cu(Im)_2(SCH_3)(S(CH_3)_2)^+$, we obtain an inner-sphere reorganisation energy of 62 kJ/mole, whereas models of the rhombic type 1 proteins nitrite reductase and stellacyanin have slightly larger values, 78 and 90 kJ/mole.

It is far from trivial to compare these values with experimental data. First, we need an estimate of the outer-sphere reorganisation energy. However, it depends strongly on the geometry of the docking complex of the donor and acceptor proteins in the electron-transfer reaction of interest, and it is unlikely that it should be additive for different reactions. Therefore, it is highly questionable to use Marcus' combination rules [6] to obtain reorganisation energies for reactions that have not been studied experimentally [102–107]. It should also be noted that the other terms in the Marcus' equation, the reduction potential and the coupling constant, also change when the docking complex is formed [108]. Therefore, reliable comparisons can only be done when calculations and experiments are performed on the same electron-transfer reaction.

However, to get a crude feeling about the relation between the calculated and measured reorganisation energies, we can proceed in the following way. The outer-sphere reorganisation energy of three tentative configurations of the dock-

ing complex between plastocyanin and its natural electron donor, cytochrome *f*, has been estimated by force-field methods and numerical solution of the Poisson–Boltzmann equation [99]. The best estimate is 42 kJ/mole, and it can be combined with our calculated inner-sphere reorganisation energy (inner-sphere reorganisation energies can to a good approximation be expected to be additive, since they do not depend on the conformation of the docking complex) for plastocyanin to get an approximate total self-exchange reorganisation energy of 100 kJ/mole. This energy is slightly lower than the experimentally measured reorganisation energy for plastocyanin (120 kJ/mole) [102]. The reorganisation energy of azurin, which is the best studied blue copper protein [103–107], is slightly lower (about 80 kJ/mole), but it is likely that azurin, with its bipyramidal copper site, has a lower reorganisation energy than the pyramidal site in plastocyanin [68].

Recently, Loppnow and Fraga [109] have estimated the reorganisation energy for plastocyanin by analysing resonance Raman intensities. They obtain an inner-sphere reorganisation energy of 18 kJ/mole, which is significantly lower than our [105]. However, it represents the reorganisation energy of *charge transfer* during the excitation to the intense blue line. As we saw above, only about 0.2 *e* is transferred during this excitation (and only from S_{Cys} to Cu) and it has therefore little to do with the reorganisation energy during electron transfer of plastocyanin [68].

We have also investigated how the blue copper proteins have achieved a low reorganisation energy. As can be seen in Figure 9, a six-coordinate $Cu(H_2O)_6^{+/2+}$ complex has a rather small reorganisation energy, 112 kJ/mole. However, Cu(I) cannot stabilise such a high coordination number. If it is allowed to relax to its preferred coordination number, the reorganisation energy of $Cu(H_2O)_6^{+}$ increases strongly, to 336 kJ/mole. If the number of ligands is lowered to four, we get a rather high reorganisation energy, 186–247 kJ/mole for $Cu(H_2O)_4^{+/2+}$, depending on whether the reduced complex is allowed to relax to a lower coordination number or not. Thus, the low coordination number of the copper ion in the proteins is unfavourable for the reorganisation energy, but necessary since Cu(I) normally does not bind more than four ligands.

Instead, the low reorganisation energy of the blue copper proteins is achieved by a proper choice of ligands. Nitrogen ligands give an appreciably (50 kJ/mole) lower reorganisation energy than water, owing to the lower Cu–N force constant. A methionine ligand gives an even lower reorganisation energy (by 14 kJ/mole), because of its weaker Cu–S bond. The cysteine ligand decreases the reorganisation energy even more, by 45 kJ/mole, although the $Cu–S_{Cys}$ force constant is appreciably higher than the one of Cu–N. This decrease is caused by the transfer of charge from the negative charged thiolate group to Cu(II), which makes the oxidised and reduced structures quite similar. The effects of the methionine and cysteine ligands are approximately additive, so the $Cu(NH_3)_3(SH)(SH_2)^{+/0}$ complex has a reorganisation energy of 74 kJ/mole. Finally, for the trigonal

$Cu(NH_3)_3(SH)(SH_2)^{+/0}$ complex (all the other complexes have been tetragonal), the oxidised structure is even closer to the reduced one, so the reorganisation energy is only 66 kJ/mole. If more realistic models are used, the reorganisation energy decreases by 4 kJ/mole and we arrive at the estimate discussed above.

Thus, we can conclude that the inner-sphere reorganisation energy of our blue copper models is similar to the one in the proteins. This indicates that the proteins do not alter the reorganisation energy to any significant degree, i.e. that protein strain is not important for the low reorganisation energies of the blue copper proteins. On the contrary, an important mechanism used by the blue copper site to reduce the reorganisation energy is the *flexible* bond to the methionine ligand, which can change its geometry at virtually no cost [54,68]. This mechanism is actually the *antithesis* of the strain hypotheses, which suggest that a low reorganisation energy is obtained by the rigid protein obstructing any change in geometry.

6. REDUCTION POTENTIALS

The reduction potential is central for the function of electron-transfer proteins, since it determines the driving force of the reaction. In particular, it must be poised between the reduction potentials of the donor and acceptor species. Therefore, electron-transfer proteins normally have to modulate the reduction potential of the redox-active group. This is very evident for the blue copper proteins, which show reduction potentials ranging from 184 mV for stellacyanin to ~1000 mV for the type 1 copper site in domain 2 of ceruloplasmin [1,110,111].

These two copper sites are untypical in that stellacyanin has a glutamine amide oxygen atom as the axial ligand (instead of methionine), whereas the ceruloplasmin centre does not have any axial ligand at all (leucine replaces the methionine ligand). However, blue copper proteins with the typical $CuHis_2CysMet$ ligand sphere have reduction potentials between 260 and 680 mV (e.g. pseudoazurin and rusticyanin) [1,63], although they share the same active site. It is also clear that the reduction potentials of the blue copper proteins are high, higher than for most other electron-transfer proteins (–700 to +400 mV for iron–sulphur clusters [112] and –300 to +470 for cytochromes [113,114]), and also higher than for a copper ion in aqueous solution (+150 mV [115]).

The reason of these high potentials and their great variation has been much discussed. Originally, the entatic state and the induced rack hypotheses suggested that the high potential was caused by protein strain. They proposed that the protein forces Cu(II) to bind in a geometry more similar to that preferred by Cu(I). Thus, Cu(II) should be destabilised, which would increase the reduction potential [10,12]. This effect has been observed for inorganic complexes with strained ligands [115].

However recently, Malmström and Gray showed that the reduction potential of denatured azurin is *higher* than for the native protein [105,116,117]. This shows that the reduced copper site gains more from unfolding than the oxidised site, especially as unfolding would increase the solvent accessibility of the site, thereby favouring Cu(II) and lowering the reduction potential. Consequently, the overall effect of the folding of the protein is a *lowering* of the reduction potential [117], i.e. opposite to what the strain hypotheses originally suggested.

This is in line with the suggestion by Solomon and co-workers that it is only the $Cu(I)–S_{Met}$ bond that is constrained by the protein [13]. A normal $Cu(I)–S_{Met}$ bond length is about 230 pm, whereas in the blue copper proteins, the observed length is around 290 pm. Such an elongation can be predicted to reduce significantly the donation of charge from the ligand to the copper ion, which would increase the reduction potential. In fact, density functional $X\alpha$ calculations indicate that the reduction potential would increase by more than 1000 mV by this elongation [13].

Malmström et al. have extended this hypothesis to include also other axial ligands [117,118]. They point out that stellacyanin has the strongest axial ligation among the blue copper proteins (a glutamine amide group at a distance of ~220 pm) and also the lowest reduction potential. Azurin has two axial ligands at distances around 310 pm and a higher reduction potential (285–310 mV). In plastocyanin, the Cu–O distance has increased to about 390 pm, as has the reduction potential (to 380 mV). In rusticyanin, the Cu–O distance is even greater, 590 pm, and the carbonyl oxygen does no longer point towards the copper site. This is correlated with a high reduction potential of 680 mV (however, they disregard the compensating shortening of the $Cu–S_{Met}$ bond in plastocyanin and rusticyanin).

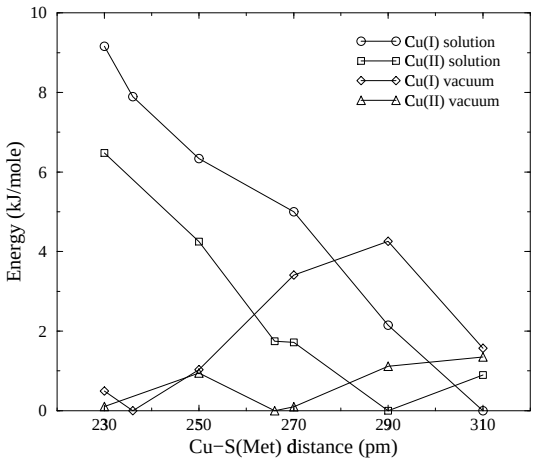

Figure 10. The calculated potential energy surface of the Cu–S_{Met} bond in the $Cu(Im)_2(SCH_3)$-$(S(CH_3)_2)^{+/0}$ complexes [35]. Two curves are given for each oxidation state, one in vacuum and one in water (calculated with the CPCM method). The actual potential in any protein can be expected to found in between these two extreme cases. Reduction potentials can be found by forming the difference between the curves of the oxidised and reduced complex together with a hypothesis whether the Cu–S_{Met} bond is constrained in the oxidised, reduced, or both states [68]. Note that 1 kJ/mole = 9.6 mV.

Finally, in fungal laccase and ceruloplasmin, which have the highest known reduction potentials (750–1000 mV), a leucine replaces the methionine ligand, yielding a three-coordinate copper site. Thus, they propose that the protein fold dictates the reduction potential of the copper site by varying the strength of the axial ligation [117,118]. We have examined these suggestions by several types of calculations.

First, we have used free energy perturbations to estimate the maximum strain energy plastocyanin or nitrite reductase can mobilise to resist a certain copper geometry [54]. These calculations show that the proteins are quite indifferent to the Cu–S_{Met} bond length. It costs less than 5 kJ/mole to change the length of this bond between the values observed in different crystal structures or in optimised vacuum models. This energy is at least a factor of two too low to explain the observed differences in the Cu–S_{Met} bond length. Instead, the difference between the calculated and observed Cu–S_{Met} bond seems to be caused by systematic errors in the theoretical method, dynamic effects, and solvation effects [26,35,54], as was discussed above.

Second, quantum chemical calculations of the potential energy surface of the Cu–S_{Met} bond shows that it costs less than 10 kJ/mole to change the Cu–S_{Met} bond length by 100 pm around its optimum value (see Figure 10), a range larger than the natural variation in this bond [14,54]. Thus, even if the proteins could constrain this bond, it would affect the electronic part of the reduction potential by less than 10 kJ/mole, or 100 mV, i.e. much less than the variation found among the blue copper proteins. Moreover, a constrained Cu(I)–S_{Met} bond would

destabilise the reduced state and therefore *decrease* the reduction potential, contrary to the suggestion of a raised potential [119] and the fact that the blue copper proteins are characterised by high reduction potentials.

However, there are other contributions to the reduction potential than the electronic part, most prominently the solvation energy of the active site caused by the surrounding protein and solvent. We have therefore studied the reduction potential of the blue copper proteins using various methods to include the solvation effects. The results have shown that constraints in the Cu–S_{Met} bond length can affect the reduction potential by less than 70 mV (c.f. Figure 10) [35].

Furthermore, we have tested the suggestion [63,118] that the reduction potential is determined by the axial backbone carbonyl ligand or by replacements of the methionine ligand (by glutamine in stellacyanin or leucine in ceruloplasmin and laccase). Again, our results show that the potential energy surfaces of the axial ligands are too soft to account for the variation in reduction potential among the blue copper proteins, even if solvation effects are taken into account (the total effect is less than 140 mV) [35]. This is in accordance with mutation studies of the axial methionine ligand in azurin [120], showing that most substitutions give only modest changes (less than 60 mV). The largest effects are found for mutations to hydrophobic residues, which increase the reduction potential by up to 140 mV, and also mutations that change the structure of the copper site [121].

Therefore, there must be other reasons for the high potentials of the blue copper proteins. Examination of small inorganic models [63,115,122] have shown that anionic ligands lower the potential, whereas sulphur and nitrogen π acceptor ligands raise the potential. Our calculations of the reduction potentials of a number of blue-copper models confirm this [45]. The replacement of an ammonia ligand in $Cu(NH_3)_4^{+/2+}$ by SH_2 increases the potential by 0.7 V, whereas SH^- decreases the potential by 0.3–0.5 V. If both models are included in the complex, $Cu(NH_3)_2(SH)(SH_2)^{0/+}$, the potential hardly change relative to the $Cu(NH_3)_4^{+/2+}$ complex. The same is true if more realistic ligands are used ($Cu(Im)_2(SCH_3)$-$(S(CH_3)_2)^{0/+}$). A tetragonal model of the rhombic blue copper proteins has a slightly larger reduction potential than the trigonal model (0.07 V), but it is not clear if this difference is significant.

Moreover, other effects are as important as the ligands. The dielectric properties of the protein matrix are very different from those of water. It has often been argued that it behaves as a medium with a low dielectric constant (around 4 compared to 80 in water) [47,123,124]. Figure 11 shows that this gives rise to a very prominent change in the reduction potential of a blue-copper site [45]. It increases by 0.8–1 V as the site is moved from water solution to the centre of a protein with a radius of 1.5 nm (like plastocyanin) or 3.0 nm (like an azurin tetramer). It can also be seen that it is not necessary to move the site to the centre of the protein to get a full effect. Already at the surface of the protein, 80% of the maximum effect is seen, and when the site is 0.5 nm from the surface (as is typi-

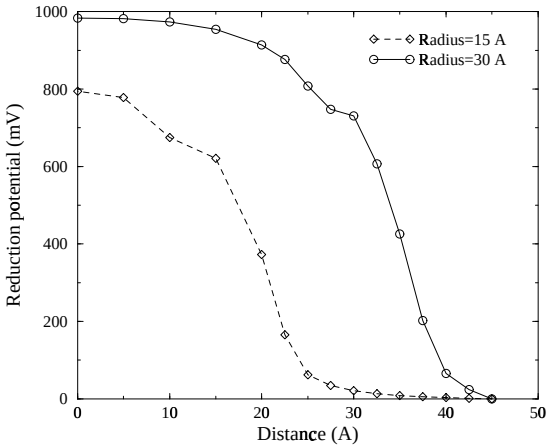

Figure 11. The reduction potential of the $Cu(Im)_2(SCH_3)(S(CH_3)_2)^{0/+}$ complex as a function of the size of the protein (1.5 or 3.0 nm radius) and the distance between the copper ion and the centre of the protein [45]. The protein was modelled by a sphere of a low dielectric constant (4) surrounded by water (ε = 78.39), and the copper site as a collection of point-charges taken from quantum chemical calculations. The potentials were calculated with the MEAD program.

cal for the blue copper proteins), the change in the reduction potential is 90% of the maximum. Thus, reduction potential of the blue-copper site in the protein will be 0.6–0.9 V higher than in water solution, in accordance with a 0.5-V variation in the cytochrome reduction potentials depending on the solvent exposure of the haem group [125]. This effect alone explains the high reduction potential of the blue copper proteins compared to copper in aqueous solution.

Naturally, details of the protein matrix, i.e. the presence and direction of protein dipoles and charged groups around the copper site, also have strong influence on the reduction potential [53,126]. In fact, a single water molecule 0.45 nm from the copper ion may change the potential by 0.2 V, and backbone amide groups may have similar effects [53]. The water accessibility and the packing of hydrophobic residues have also been shown to significantly influence the reduction potential. In fact, it has been suggested that the protein may modify the reduction potential by more than 1 V without any changes in the redox-active group [52]. With these results in mind, the large variation of the reduction potentials of blue copper proteins is not surprising, even if the detailed mechanism remains to be revealed for most proteins [45,53,126].

7. RELATED PROTEINS

7.1 The binuclear Cu_A site

Cytochrome *c* oxidase is the terminal oxidase in both prokaryotic and eukaryotic cells and is responsible for the generation of cellular energy via oxidative phosphorylation [127]. It couples the catalytic four-electron reduction of O_2 to

water to transmembrane proton pumping, which can be used for ATP synthesis and long-range electron transfer. The active site is a haem a_3–Cu_B binuclear site, whereas a second haem *a* and an additional copper site, Cu_A, serve as electron-transfer intermediates between cytochrome *c* and the active site. The Cu_A site shows many similarities with the blue copper proteins. Recently, the structure of cytochrome *c* oxidase was determined by crystallography [128–130]. This solved an old controversy regarding the geometry of the Cu_A site [131,132], showing that it is a binuclear site, bridged by two cysteine thiolate groups. Each copper ion is also bound to a histidine group and a weaker axial ligand, a methionine sulphur atom for one copper and a backbone carbonyl group for the other. The Cu–Cu distance is very short, ~245 pm [133], and it has been speculated that it represents a covalent bond [134–136]. A similar site is found in nitrous oxide reductase, a terminal oxidase that converts N_2O to N_2 in denitrifying bacteria [137].

During electron transfer, the Cu_A site alternates between the fully reduced and the mixed-valence (Cu^I+Cu^{II}) forms. Interestingly, the unpaired electron in the mixed-valence form seems to be delocalised between the two copper ions. Several theoretical investigations of the electronic structure and spectrum of the Cu_A dimer have been published [138–144]. In similarity to the blue copper proteins, it has been suggested that the structure and the properties of the Cu_A site is determined by protein strain. More precisely, it has been proposed [136] that Cu_A in its natural state is similar to an inorganic model studied by Tolman and coworkers [145]. This complex has a long Cu–Cu bond (293 pm) and short axial interactions (~212 pm). The protein is said to enforce weaker axial interactions, which is compensated by shorter bonds to the other ligands and the formation of a Cu–Cu bond. This should allow the protein to modulate the reduction potential of the site [136,146].

We have studied the structure, reorganisation energy, and reduction potential of the Cu_A site with the same theoretical methods as for the blue copper proteins [147]. The experimentally most studied state of Cu_A is the mixed-valence state. Our optimised structure of $(S(CH_3)_2)(Im)Cu(SCH_3)_2Cu(Im)(CH_3CONHCH_3)^+$ is very similar to available experimental data [128–130,133,148–151] (c.f. Figure 12 and Table 6). The Cu–Cu distance is 248 pm, 2–5 pm longer than what is obtained by extended x-ray absorption fine structure measurements (EXAFS), and the Cu–S_{Cys} distances are 231–235 pm (~2 pm longer than the EXAFS results). Even the distances to the axial ligands are within the experimentally observed range: 245 pm for the methionine ligand and 220 pm for the backbone carbonyl group. The difference in the Cu–N_{His} distances seems to be slightly larger, 6–7 pm, which is probably due to hydrogen-bond interactions in the protein [147].

It has been noted that some inorganic models of the Cu_A site have an appreciably longer Cu–Cu distance (~290 pm) [145]. This is accompanied by a change in the electronic state: In the proteins there is a σ^* antibonding interaction between

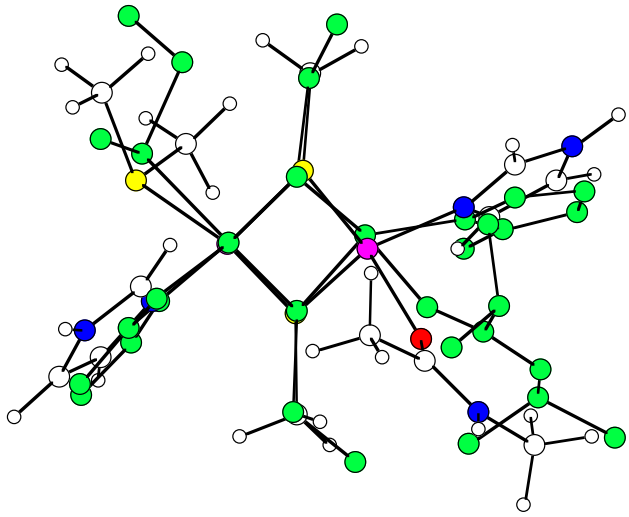

Figure 12. The optimised geometry of the σ-bonded structure for the $(S(CH_3)_2)(Im)Cu(SCH_3)_2Cu(Im)(CH_3CONHCH_3)^+$ complex [147] compared to the crystal structure of the Cu_A site in cytochrome *c* oxidase (shaded and without any hydrogen atoms) [149].

the copper ions in the singly occupied orbital (an orbital of B_{3u} symmetry for an idealised D_{2h} Cu_2S_2 core), whereas in the model, there is instead a Cu–Cu π bonding interaction (B_{2u} symmetry) [136,138,141,143]. We have also optimised the π bonded electronic state. It is characterised by a Cu–Cu bond length of 310 pm and a slightly larger variation in the Cu–S_{Cys} distances (226–236 pm), whereas the other geometric parameters are similar to those of the σ bonded structure. In particular, there is no significant difference in the bond lengths to the axial ligands. Therefore, it is unlikely that variations in the axial interactions (caused by the protein) may change the electronic state of Cu_A.

Interestingly, the two structures are almost degenerate; they have the same energy within 2 kJ/mole. In fact, the full potential surface for the Cu–Cu interaction is extremely flat. As can be seen in Figure 13, the barrier between the two electronic states is less than 5 kJ/mole and the Cu–Cu distance can vary over 100 pm (240–340 pm) at a cost of less than 5 kJ/mole both in vacuum and in water solution. Thus, there is no indication that the Cu_A site should be significantly strained. The difference between the protein structures and the mixed-valence model is caused by the degeneration of the two electronic states (indicating that small differences in the surrounding protein may stabilise either structure) and the fact that the inorganic complex involve poor models of the histidine and axial ligands (four amine groups at almost the same distances, 211–212 pm). This illustrates the danger of relying on inorganic complexes with poor ligand models; if such models had been used in theoretical calculations, nobody had believed in them.

The two electronic states differ in the localisation of the unpaired electron: in the σ* state, the electron is delocalised over the whole system, whereas in the π state, the electron is more localised to one copper. Our calculations reproduce this movement of the electron: in the system with a long Cu–Cu bond, the elec-

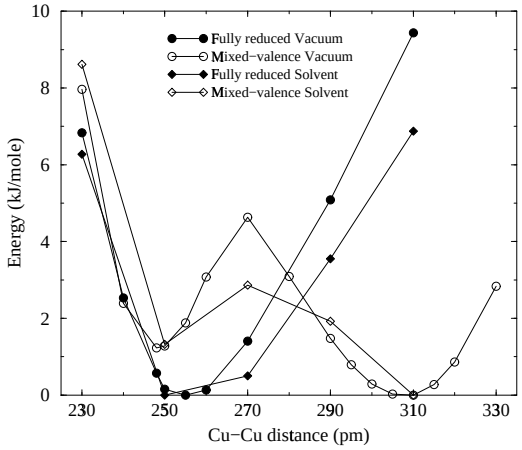

Figure 13. The calculated potential energy surface for the Cu–Cu interaction of the $(S(CH_3)_2)$-$(Im)Cu(SCH_3)_2Cu(Im)(CH_3CONHCH_3)^+$ complex in vacuum and in water [147].

tron is mainly localised to the copper ion with the methionine ligand. However, the electronic structure is quite flexible, as experiments with engineered Cu_A sites have shown [146,153,154].

The optimum structure of the fully reduced state of our Cu_A model is also shown in Table 6. It can be seen that most Cu–ligand bond lengths increase by 1–7 pm upon reduction, but the Cu–Cu distance increases by 9 pm and the Cu–O distance by as much as 30 pm. No crystal structure has been published for this oxidation state, but EAXFS data are available [133]. It can be seen in Table 6 that our optimised structure is quite close to these results, with the same trends as for the mixed valence structure (i.e. slightly too long Cu–Cu and Cu–N bonds). Therefore, our calculations excellently reproduce the changes upon reduction observed by EXAFS, e.g. the change in the Cu–Cu distance. We also reproduce the larger variation in the Cu–S distances (233–247 pm). Consequently, the calculated reorganisation energies can be expected to be quite accurate.

For the reduction of the σ^* state, we predict a self-exchange inner-sphere reorganisation energy of 43 kJ/mole [147]. This is 20 kJ/mole lower than for plastocyanin [68]. It has been speculated that the reorganisation energy of Cu_A should be half as large as for a blue-copper site due to the delocalised electron [136,144, 155,156] and older estimates of the reorganisation energy of the Cu_A were in general quite low, 15–50 kJ/mole [157,158]. However, recent experiments have indicated that the reorganisation energy is of the same size as for the blue copper proteins, around 80 kJ/mole [159]. If the outer-sphere reorganisation energy of cytochrome *c* oxidase is of the same magnitude as for plastocyanin (~40 kJ/mole [99], our calculated reorganisation energy is in good agreement with the latter experiment. The reorganisation energy for reduction of the π state is appreciably higher, 69 kJ/mole, which is due to the change in the Cu–Cu bond length and the angles in the CuS_2Cu core [147].

Table 6. Bond distances in four electronic states of the $(S(CH_3)_2)(Im)Cu(SCH_3)_2Cu(Im)$-$(CH_3CONHCH_3)$ model [147] compared to experimental data for Cu_A and model compounds.

Oxidation states	Electronic State	Distances (pm)				
		Cu–Cu	$Cu–S_{Cys}$	$Cu–N_{His}$	$Cu–S_{Met}$	Cu–O
I+I		257	233–247	207–211	240	250
	EXAFS[a]	251–252	231–238	195–197		
II+I	σ*	248	231–235	202–209	245	220
	π	310	227–236	203–210	242	219
	EXAFS[a]	243–246	229–233	195–203		
	crystal[b]	220–258	207–244	177–211	239–302	219–300
	model[c]	293	225–229	211	212	212
II+II		342	228–234	202–203	242	202
	model[d]	334	233	206	210–226	210–226

[a] EXAFS data [133,151].

[b] Protein crystal structures [128-130,148-150].

[c] A mixed-valence inorganic model synthesised by Tolman and coworkers [145] with a π ground state. Note that both the histidine and axial ligands are amine groups in the model.

[d] Another fully oxidised inorganic model synthesised by Tolman and coworkers [152]. Note that each copper ion is five-coordinate with three amine nitrogen ligands.

The potential energy surface for the Cu–Cu bond in the reduced Cu_A model is almost as flat as in the mixed-valence state (Figure 13). Therefore, the reduction potential of the Cu_A site cannot change by more than 100 mV by constraints in this bond. In particular, a change in the electronic structure of the mixed-valence state from π to σ does not change the reduction potential by more than 13 mV. Solvation effects alter the results by less than 20 mV (Figure 13).

Similarly, the potential energy surfaces of the $Cu–S_{Met}$ and Cu–O bonds are also flat (Figure 14). The two bond lengths can vary over a range of almost 100 pm at an energy cost of less than 8 kJ/mole. As for the blue copper proteins, the optimum distance for the carbonyl group is shorter than for the methionine ligand. Thus, it unlikely that the axial ligands determine the reduction potential of the Cu_A site [136,146,155]. Even if the protein could constrain these distances, the results in Figure 14 show that the reduction potential would vary by less than 80 mV for the experimentally observed range of these bond lengths. Inclusion of solvation effects does not change the situation significantly [147].

Finally, we have also studied the fully oxidised Cu_A model (Cu^{II}+Cu^{II}). This state has not been unambiguously observed in biology yet, but it has been suggested that it is responsible for the differing characteristics of the Cu_Z site in nitrous oxide reductase [146,160]. Our calculations indicate that the fully oxidised state should have a much longer Cu–Cu bond (342 pm) and a shorter Cu–O bond (202 pm) than the mixed-valence state. This is reasonably similar to a fully oxidised inorganic model complex with bridging thiolate groups and three amine nitrogen ligands of each copper, see Table 6 [152]. In particular, the angles in the CuS_2Cu core are very similar, 85° compared to 83° for the S–Cu–S angle. This is quite different from the angles in the mixed-valence σ* state (115°). Therefore,

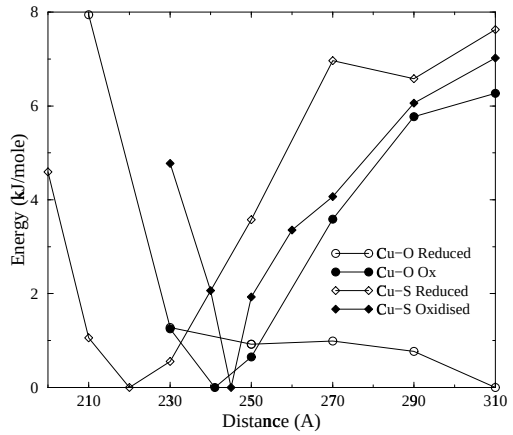

Figure 14. The calculated potential energy surfaces for the Cu–S_{Met} and Cu–O interactions of the $(S(CH_3)_2)(Im)Cu(SCH_3)_2Cu(Im)(CH_3CONHCH_3)^+$ complex in vacuum [147].

the self-exchange reorganisation energy for the oxidation of this state is high, 133 kJ/mole [147].

Interestingly, the π-bonded structure is more similar to the fully oxidised state, and the corresponding reorganisation energy is also appreciably lower, 90 kJ/mole. It has been suggested that the Cu_A and Cu_Z sites in nitrous oxide reductase in fact are the same site, with altered properties as a result of a conformational change [146,160]. If this suggestion is correct, it follows from our results that the conformational change may stabilise the σ* structure in the Cu_A site, but the π structure in the Cu_Z site. This would hardly cost anything in energy terms (Figure 13), but it would strongly reduce the inner-sphere reorganisation energy for oxidation of the mixed-valence state [147].

In conclusion, the properties of the Cu_A dimer are very similar to those of the blue copper proteins. Each copper ion has a trigonal structure with a weakly bound axial ligand. There are two nearly degenerate electronic states, which together with the flat potential of the axial ligands give a very plastic site. The inner-sphere reorganisation energy is slightly lower than for the blue copper proteins and it is achieved by the same mechanisms: delocalisation of the charge between the copper and sulphur ions and flexible bonds to the axial ligands. As for the blue copper proteins we have not seen any evidence for protein strain in the Cu_A site.

7.2 Cytochromes

In nature there are only two major types of electron-carrier sites in addition to the blue copper proteins and the Cu_A site, viz. cytochromes and iron–sulphur clusters [161,162]. The cytochromes consist of an iron ion bound to a porphyrin ring. Two axial ligands complete the octahedral coordination sphere. During electron transfer, iron alternates between Fe(II) and Fe(III). Several types of cytochromes exist in biological systems, depending on the substituents on the por-

phyrin ring, the axial ligands, and the number and arrangement of the haem groups in the protein (cytochromes *a*, *b*, *c*, *f*, etc) [163]. Their reduction potential ranges between –300 and +470 mV [113,114].

Several groups have tried to predict the reduction potentials of various cytochromes using theoretical approaches [51,95,97,114,164–171]. A few groups have also studied the reorganisation energy of these proteins. For example, the outer-sphere reorganisation energy of cytochrome *c* has been calculated to 28–100 kJ/mole with various theoretical methods [6,51,93,95,97,100]. The majority of this energy comes from the protein, 70–90 %. It is also clear that the protein reduce the reorganisation energy compared a haem group in water solution, which has been estimated to 100–160 kJ/mole [95,97,100].

The inner-sphere reorganisation energy of the cytochromes is considered to be low, ranging from negligible to 48 kJ/mole [6,51,93,95,97]. It is normally estimated from the difference between the measured total self-exchange reorganisation energy and the calculated outer-sphere reorganisation energy. Considering the large variation of the latter, and an almost equally large span of experimental estimates (e.g. 70–140 kJ/mole for the self-exchange reorganisation energy of cytochrome *c* [172–174]), such estimates much be considered very approximate. Alternatively, the inner-sphere reorganisation energy has been estimated from vibrational frequencies and the observed changes in the haem geometry in crystal structures. However, also these estimates are approximate, since the observed changes in the bond lengths to the iron ion are smaller than the uncertainty in the crystal structures.

Therefore, we have investigated the inner-sphere reorganisation energy of iron porphine (the porphyrin ring without any substituents) with different axial ligands [24]. The results presented in Table 7 show that if the axial ligands are uncharged, the reorganisation energy is small, 5–9 kJ/mole, appreciably smaller than for the blue copper proteins (62 kJ/mole). It varies somewhat with the axial ligands. Two methionine ligands (as in bacterioferritin [175]) give the lowest reorganisation energy, whereas the most common sets of ligands (His–His and His–Met, as in the *b* and *c* type cytochromes [163]) give slightly higher reorganisation energies.

We have also tested a number of charged axial ligands, which have been suggested to be present in haem proteins [113]. These models have appreciably higher reorganisation energies, ranging from 20 kJ/mole (His–Cys) to 47 kJ/mole (His–Tyr). Interestingly, the only combination that has been unambiguously observed in a cytochrome is His–Tyr (in the d_1 domain of cytochrome cd_1 nitrite reductase [176]). At a first glance the results may indicate that the Tyr ligand in this cytochrome should be protonated. Yet, the reorganisation energy is not larger than observed for blue copper proteins or iron–sulphur clusters [24,68,147], so it cannot be excluded that the Tyr ligand is deprotonated. All other characterised proteins with negatively charged axial ligands are enzymes with a catalytic func-

Table 7. Geometries and inner-sphere reorganisation energies for a number of cytochrome models calculated by the B3LYP method [24]. The haem group was modelled by Fe(porphine) and Met, His, Amt (amino terminal), Cys, Tyr, and Glu were modelled by $S(CH_3)_2$, Im, CH_3NH_2, SCH_3^-, $C_5H_6O^-$, and CH_3COO^-, respectively. All complexes were assumed to be in the low-spin state in accordance with experiments [162].

Axial ligands		Oxidation	Reorg. energy	Distance to Fe (pm)		
1	2	state	(kJ/mole)	Ligand 1	Ligand 2	N
Met	Met	II	2.7	240	240	202
		III	2.1	240	240	202
His	Met	II	4.2	203	243	202
		III	4.1	200	244	201
His	His	II	3.7	205	205	202
		III	4.5	202	203	201
His	Amt	II	4.2	203	208	202–203
		III	4.4	200	205	201–202
His	Cys	II	9.7	211	238	202
		III	10.3	215	222	201–203
His	Tyr	II	21.2	206	199	202–203
		III	25.8	207	184	201–203
His	Glu	II	13.0	205	199	202–203
		III	13.4	207	187	201–202

tion rather than electron carriers (often in combination with a five-coordinate iron ion).

Much experimental data are available for the structure of small inorganic haem models with various axial ligands [177,178]. From these, it can be conclude that our calculated Fe–N_{Por}, Fe–N_{His}, Fe–S_{Met}, and Fe–S_{Cys} distances are slightly too long, by 2–3, 4–5, 6, and 3 pm, respectively [24]. This probably reflects the accuracy of the B3LYP method. However, it is also clear that the discrepancy is the same (within 1 pm) for the two oxidation states. Therefore, the *change* in the Fe–ligand bond lengths upon reduction is accurately reproduced in our models, so calculated reorganisation energies can be expected to be quite reliable. It is also notable that the accuracy of our optimised models is better than what can be expected for a metal site in protein crystallography [179]. Therefore, it is not meaningful to calibrate our results by comparing to a single protein structure.

We have also investigated how the cytochromes have achieved a low reorganisation energy [24], using similar methods as for the blue copper proteins [68]. First, an octahedral geometry is favourable for electron transfer, since there is no change in the angles upon reduction. Second, cytochromes employ nitrogen and sulphur ligands, which form weaker bonds with smaller force constants than oxygen ligands (the reorganisation energy of $Fe(NH_3)_6$ is a third of that of $Fe(H_2O)_6$). Third, covalent *strain* in the porphyrin ring decreases the changes in the Fe–N_{Por} distances. For example, if the porphyrin ring is replaced by two molecules of diformamidate ($NHCHNH^-$), a small ligand that often has been used as a reasonable minimal model for the porphyrin ring [180], the equatorial Fe–N_{Por} distances

change by 9–10 pm upon reduction, compared to ~1 pm with the full porphine model. This increases the reorganisation energy by 44 kJ/mole.

It is informative to compare the haem group and the blue copper proteins since we have argued strongly against a reduction of the reorganisation energy by strain in the blue copper proteins [10,12,14,49,63]. The major difference is that the porphyrin ring is held together by strong covalent bonds and is constrained by the aromaticity of the ring, whereas in the protein, the ligands are oriented by weak torsional constraints and non-bonded interactions. Covalent bonds are stronger than metal–ligand bonds, whereas torsions and non-bonded interactions are weaker. Therefore, the iron ion is constrained in the haem group, whereas it is more likely that the protein will distort if the preferences of the metal and the protein differ. Moreover, it must be recognised that if significant strain were involved in the binding of a metal, it would simply not bind; a strain energy of 70 kJ/mole, as has been suggested for the blue copper proteins [12], corresponds to an equilibrium constant of $1.5 \cdot 10^{12}$.

7.3 Iron–sulphur clusters

Iron–sulphur clusters are the third type of the widely available electron-transfer sites in biology. They consist of iron ions surrounded by four sulphur ions, either thiolate groups from cysteine residues or inorganic sulphide ions. Regular clusters with one (rubredoxins), two, three, or four (ferredoxins) iron ions are known, as well as a number of more irregular clusters, also with other ligands than cysteine [112,181]. Their reduction potentials vary between –700 and +400 mV [112].

The electronic structure, spectroscopy, and reduction potential have been thoroughly studied for all common classes of iron–sulphur clusters [52,89,182–191]. In particular, Noodleman and coworkers have performed detailed quantum chemical calculations on iron–sulphur clusters in various spin states [192–198]. It is now settled that rubredoxin contains an iron ion in the high-spin state (quintet for Fe^{II}, sextet for Fe^{III}), whereas in the [2Fe-2S] clusters, the two iron ions are both in the high-spin state, but antiferromagntically coupled to form a singlet or doublet state for the oxidised (III+III) and reduced (mixed-valence II+III) forms, respectively [112,162]. In variance to the Cu_A site, the unpaired spin is trapped at one of the iron ions in the mixed-valence state.

However, nobody seems to have studied the reorganisation energy of the iron–sulphur clusters systematically. Therefore, we have initiated an investigation of the inner-sphere reorganisation energy of $Fe(SCH_3)_4$, $(SCH_3)_2FeS_2Fe(SCH_3)_2$, and $(SCH_3)_2FeS_2Fe(Im)_2$ [24]. The optimised structures and the calculated inner-sphere reorganisation energies are collected in Table 8.

The Fe–S distances in the $Fe(SCH_3)_4$ model increase from 232 to 242 pm when the site is reduced. This 10-pm increase is similar to what is observed in inorganic model complexes, but the average distances are shorter in the models, 227 and 236 pm, respectively [199]. Thus, the Fe–S distances are again 5–6 pm too

Table 8. Geometries and inner-sphere reorganisation energies for iron–sulphur models calculated by the B3LYP method [24].

Model	Oxidation state	Reorg. energy	Distance to Fe (pm)			
			S_{Cys}	S_i	Fe	N_{His}
$Fe(SCH_3)_4$	II	21.4	242			
	III	18.3	232			
Models [199]	II		232–238			
	III		225–228			
Proteins [202,203]	II		224–236			
	III		223–233			
$(SCH_3)_2FeS_2Fe(SCH_3)_4$	II+III	34.3	245–249	225–241	299	
	III+III	41.1	235–237	226–227	285	
Models [204]	III+III		230–231	219–223	270	
Proteins [205]	III+III		222–237	211–228	260–278	
$(SCH_3)_2FeS_2Fe(Im)_2$	II+III	18.3	233–239	225–229	271	216–220
	III+III	21.8	227–232	219–230	275	210–212
Proteins [206,207]	II+III		222–231	223–235	271	213–223

long, but the change during oxidation is well reproduced. However, in the protein, the distances seem to be even shorter, 226 and 232 pm according to EXAFS experiments, and the change is smaller [112,200]. This is probably an effect of the protein environment, where several backbone amide groups form hydrogen bonds to the S_{Cys} atoms [76,201]. COMQUM calculations on rubredoxin show that the protein reduces the calculated average Fe–S distances to 230 and 236 pm for the oxidised and reduced site, respectively [24]. Thus, the hydrogen bond reduce the bond length more in the reduced than in the oxidised complex, giving an excellent agreement with experiments for the change in the bond length upon reduction.

The calculated inner-sphere reorganisation energy of the $Fe(SCH_3)_4$ model in vacuum is 40 kJ/mole. In the proteins the hydrogen bonding reduce the reorganisation energy by ~12 kJ/mole [24]. The inner-sphere reorganisation energy of rubredoxin has been estimated from the change in Fe–S bond lengths and the corresponding vibrational frequency [208]. The result is ~10 kJ/mole lower than our estimate, which illustrates that the reorganisation energy does not only arise from the changes in these bond lengths.

We have also studied the $(SCH_3)_2FeS_2Fe(SCH_3)_2$ complex in its fully oxidised and mixed-valence form as a model of the [2Fe-2S] ferredoxins. The optimised Fe–S distances are 5–10 pm longer than in experiments, again reflecting the systematic error of the B3LYP method. The discrepancy for the Fe–Fe distance is slightly larger, but this is probably an effect of a flexible Fe–Fe interaction, as for the Cu–Cu bond in the Cu_A site [147]. Our calculated reorganisation energy is 75 kJ/mole, appreciably larger than for the rubredoxin site. This is in accordance with a lower rate of electron transfer for these sites in proteins as well as in model systems [162,204].

At first, the increase in reorganisation energy for the dimeric iron–sulphur clusters (compared to the monomeric rubredoxin site) may seem a bit strange,

considering that for the dimeric Cu_A site, the reorganisation energy decreased compared to the blue-copper monomer. The reason for this behaviour is that the unpaired electron in the mixed-valence iron–sulphur site is localised to one of the iron ions, whereas it is delocalised in the Cu_A site. It has been suggested that a delocalised dimer should have approximately half the reorganisation energy of the monomer, because of a reduction in the change in the bond lengths upon reduction by a factor of two [144,155,156]. This was essentially what we observed for the Cu_A site [147]. In the iron–sulphur dimers, the change in the bond lengths upon reduction is not significantly altered. In fact, it is slightly increased around the iron ion that is reduced (13 pm compared to 9 pm for the rubredoxin model), but there are also appreciable changes around the other iron ion (6 pm on average). Even if the force constants are reduced around the reduced iron ion, the number of bonds is doubled. Therefore, the total reorganisation energy of the ferredoxin model increases.

Interestingly, our model of the Rieske iron–sulphur site, $(SCH_3)_2FeS_2Fe(Im)_2$, has an appreciably lower reorganisation energy, 40 kJ/mole. This is due to smaller changes around the iron ions, 2–8 pm (c.f. Table 8) and lower force constants of the imidazole ligands. As for the cytochromes and blue copper proteins, we have also investigated how the iron–sulphur clusters have achieved a low inner-sphere reorganisation energy. First, iron is a better ion than copper, since the Fe(II) and Fe(III) have similar preferences for the geometry and coordination number. Moreover, even at a fixed geometry, copper gives a higher reorganisation energy than iron. For example, the reorganisation energy of an octahedral $Cu(H_2O)_6$ complex is twice as large as for $Fe(H_2O)_6$. This probably reflects the difference in the charge of the two ion pairs. Second, four ligands give slightly lower reorganisation energies than six, provided that the geometry does not change, since there are fewer bonds. Finally, iron–sulphur sites employ soft and large thiolate ligands, which give smaller reorganisation energies than harder ligands such as water.

8. PROTEIN STRAIN

The suggestion that proteins use mechanical strain for their function is an old but still viable hypothesis [12,10,209–211]. The most classical example of a protein for which strain has been suggested to play a functional role is probably lysozyme [212]. It was originally suggested that this protein forces its substrate to bind in an unfavourable conformation, viz. a conformation similar to the transition state. However, theoretical calculations by Levitt and Warshel convincingly showed that strain has a negligible influence on the rate of this enzyme; instead, the catalytic power is gained by favourable electrostatic interactions in the transition state [50]. This and other cases have led several leading biophysical chemists

to argue strongly against strain as an important factor in enzyme catalysis [50, 213,214].

To make strain hypotheses testable, it is vital to define what is meant by strain. Warshel has defined strain as distortions caused by covalent interactions (bond, angles, and dihedrals) and possibly also the repulsive part of the Van der Waals interaction [50]. This is close to the intuitive conception of mechanical strain, but it is hard to estimate except in classical simulations of proteins. We have used a wider definition of strain [49]: a change in geometry of a ligand (e.g. a metal coordination sphere) when bound to a protein (it includes effects that normally are not considered as mechanical strain, most prominently electrostatic and solvation effects). This change must be relative to a reference state. We have used the vacuum geometry as the strainless state, but other reference states are also conceivable, e.g. the ligand in water solution. However, such a choice is less well-defined. For example, how large changes should be allowed in the reference state: May the number of ligands change? May a water molecule come in as an axial ligand, or as an equatorial ligand, or may it even replace the protein ligands?

It must be recognised that any ligand necessarily acquires slightly different properties when bound to a protein. This is an effect of the trivial fact that a protein is different from vacuum or solution (it has another effective dielectric constant and presents specific electrostatic interactions). Such changes have been estimated for a number of protein–ligand complexes, and Liljefors et al. have argued that the energies involved are less than 13 kJ/mole if the reference state is the ligand in solution [215]. If the reference state instead is the ligand in vacuum, appreciably larger energies are observed. We have, for example, calculated energies associated with the change in geometry of the metal site when inserted from vacuum into a protein to 30–60 kJ/mole for the catalytic and structural zinc ions in alcohol dehydrogenase [75–77] and similar values for the blue copper proteins and iron–sulphur clusters, 16–51 kJ/mole [24,26]. We suppose that the strain hypotheses are intended to deal with systems where the strain is larger than normal and has a functional role. Therefore, we consider distortions smaller than this insignificant, unless there is a clear function of the strain [49].

Originally, the entatic state and the induced rack theories for the blue copper proteins discussed only the rigid protein and the strained cupric conformation, i.e. mechanical strain. However, lately they have started to embrace virtually any modifying effect of the protein. For example, in a recent commentary [63], Gray, Malmström and Williams consider exclusion of water as a “constraining factor”. This is a most unfortunate widening and blurring of the concept, making discussions harder. Moreover, seen in that way, all proteins are strained or entatic (i.e. they are adapted to functional advantage [63]), but at the same time such a hypothesis becomes void of any predictive value.

With Warshel’s or our definition of strain, we have shown without any doubts that the cupric structure of the blue copper proteins is not strained to any signifi-

cant degree [14,33,34], especially if the dynamics at ambient temperatures and the dielectric surroundings of the copper site are considered [26,35,45,54]. The electronic structure explains why protein sites with a cysteine ligand have structures close to a tetrahedron, whereas inorganic complexes are tetragonal [65]. Furthermore, our and other groups have shown that the unusual spectroscopic properties and the high reduction potential of the blue copper proteins are a natural consequence of the covalent nature of the bond between copper and the cysteine thiolate group [33–36,65,83–86,96,119,216]. Similarly, we have shown that the low reorganisation energy is also intrinsic to the blue copper site [26,68]. Clearly, strain is not needed to explain any of the unusual properties of the blue copper proteins and there is no indication that mechanical strain has any functional value for the proteins.

The similarity in structure between the oxidised and reduced forms of the blue copper proteins has often been taken as an argument for the strain hypotheses [63]. However, our results show that this is a natural effect of the copper ligands, especially the cysteine ligand [14]. Likewise, the similarity between metal-substituted blue copper proteins and their native counterparts has been taken as an argument for strain [63,217]. Yet, there is an appreciable variation in the metal–ligand distances for the various proteins, viz. 43, 31, 102, and 103 pm for the bonds to N, S_{Cys}, O, and S_{Met}, respectively [63]. This points to a plastic, rather than rigid, metal site. Moreover, the changes reflect the softness of the metal, showing that the metal, rather than the protein, determines the geometry of the site. Similarly, *in trans* mutations of the copper ligands in azurin have provided strong experimental evidence for a flexible copper site [218].

The fact that the structure of the copper-free form of the blue copper proteins is similar to that of the metal-loaded form has also frequently been taken as an argument for strain. However, this does not show that the copper site is strained. Instead, it may facilitate metal binding [14,77]; if the metal chelating site was not present before the metal is bond, clearly metal binding would be harder [14,144]. Moreover, the copper-free structure is stabilised by several favourable hydrogen bonds [219–221], showing that the structure is not unnatural. In fact, there is another structure of the apo-azurin [57], in which a water molecule occupies the metal site, leading to appreciable changes in the geometry of the site. Again, this points to a substantial flexibility of the metal site.

A fourth argument for the strain hypotheses is the problem to synthesise small inorganic models that reproduce the geometry and macroscopic properties of the blue copper proteins [66,67]. The most successful models involve strained ligands [222] and the first trigonal model was reported only very recently [223]. However, inorganic modelling of blue-copper sites is full of practical problems [224]. Most prominently, Cu(II) and thiolate ligands tend to disproportionate to form Cu(I) and disulphide. In the proteins, this reaction is inhibited by the bulk of the protein. Second, our calculations show that the stability of trigonal and

tetragonal Cu(II) complexes depends strongly on the ligands. A thiolate ligand is not enough to stabilise a trigonal structure; another weak ligand, such as methionine must also be present [65]. In fact, there are still no small inorganic model that have the same set of ligands ($N_2S^-S^0$) as the blue copper proteins [66,67].

Another problem with small models is that molecules from the solution (e.g. water) may come in and stabilise tetragonal structures and higher coordination numbers [224]. It is illustrative that very few inorganic complexes reproduce the properties of the blue copper proteins [66,67], whereas typical blue-copper sites have been constructed in several proteins and peptides by metal substitution, e.g. insulin, alcohol dehydrogenase, and superoxide dismutase [66]. This shows that the problem is more related to protection from water and dimer formation than to strain.

This does not mean that the protein is unimportant for the function of the blue copper proteins. On the contrary, the protein provides the proper ligands to the copper site and protects it from unwanted ligands. This may also involve a restriction of the number of ligands of the copper ion. Typically, Cu(II) binds 4–6 ligands, whereas Cu(I) prefers 2–4, but with the bulky, soft, and negatively charged sulphur ligands, the two oxidation states accept the same coordination number. Second, the protein modifies the dielectric properties of the surroundings of the copper site, thereby reducing the outer-sphere reorganisation energy and modulating the reduction potential of the copper site. Third, the protein offers a proper path or matrix for electron transfer and the docking sites for the donor and acceptor proteins [144].

Clearly, the blue copper proteins also modulate the geometry of the copper site. The rhombic type 1 proteins stabilise a tetragonal structure, whereas the axial type 1 proteins stabilise the trigonal structure of the same copper coordination sphere. However, the energy needed for such a stabilisation, <7 kJ/mole [34], is less than the typical distortion energies occurring in all proteins due to the subtle mismatch between the protein and the ligand sphere [57,75–77,215]. Furthermore, the forces leading to such a stabilisation include electrostatics and other factors usually not defined as mechanical strain, and the functional value of this stabilisation is unclear since both types of sites are present in proteins with a similar function.

In conclusion, we have in a series of investigations addressed the function and properties of the blue copper proteins. We have emphasised the importance of defining what is meant by the strain and to discuss strain in quantitative terms. For such an investigation, theoretical methods seem to be better suited than experiments, since they directly give the energy and allow the energy to be divided into contributions from different degrees of freedom. We have in no case found any indication of a functional role for strain in the blue copper proteins. On the contrary, copper complexes in vacuum seem to have mostly the same properties as in the proteins. The proteins have constructed a metal coordinating site which

minimises the electron-transfer reorganisation energy by an appropriate choice of metal ligands, viz. ligands that are a compromise between those preferred by the Cu(I) and Cu(II) ions. In particular, the cysteine ligand is crucial, giving rise to rather tetrahedral structures (either trigonal or tetragonal). Moreover, the methionine ligand gives a very flexible bond, which can change considerably at a small expense of energy. Thus, in our eyes, strain hypotheses for the blue copper proteins are a case for Ockham's razor.

9. CONCLUDING REMARKS

We have in recent years seen an exciting development of theoretical methods for the use in biochemistry and this trend can be expected to continue with an increasing pace in the future. The background is the explosive increase in computer power and development of methods and software that can deal with large molecules at reasonable costs. Density functional methods, in particular, have become a viable tool for studies of ground-state properties. We have used them to obtain geometries. The geometries have been calibrated by comparisons with accurate crystal structures of model complexes and EXAFS data. Typically, metal distances to sulphur are ~6 pm too long, whereas distances to histidine ligands are ~4 pm too long. Such an accuracy is better than what is normally obtained by protein crystallography [179]. Moreover, errors in the calculated structures are systematic, so *differences* in geometries are accurately reproduced (within 1 pm).

Naturally, geometry optimisations of small models in vacuum necessarily ignore effects of the surroundings, e.g. hydrogen bonds, hydrophobic interactions, and steric effects, which determine torsion angles of the complexes in the protein, and also may determine the length of weak axial bonds, such as the Cu–S_{Met} bond. Therefore, geometry optimisation methods, which include the full detail of the surroundings [26,60], or even the crystallographic raw data [225], are most promising, even if they are more demanding.

Multiconfigurational second-order perturbation theory (CASPT2) has been used to obtain accurate energies and to study electronic spectra of the proteins. The results are surprisingly accurate and have been used to explore the relation between structural and spectroscopic properties. However, one should bear in mind all uncertainties inherent in the comparison of the theoretical and experimental data. The CASPT2 method itself has a well-documented uncertainty in computed excitation energies of up to 2 500 cm^{-1} [28]. To this should be added deficiencies in the basis set and the effect of the protein and solvent, which was described by a rather primitive point charge model. The significant influence of the protein on the spectroscopic properties is interesting and calls for a more accurate investigation. Preliminary results indicate that most of the effect comes from a few atoms near S_{Cys}. Thus, the effect strongly depends on the charge of

these atoms. This means that it would be enough to improve the model of a few residues near to the copper site. These residues may, for example, be modelled by higher electrostatic moments calculated at the actual conformation and environment in the protein.

Thus, it is clear that the surrounding protein and solvent have an important influence on the structure and spectra of the copper sites. For reduction potentials and outer-sphere reorganisation energies, these effects are of the same magnitude as the electronic effects and therefore essential. We have used three different levels of approximations for these effects: an array of point charges, continuum models, and combined quantum chemical and classical simulations. We anticipate that this will be an area of intensive development in the future.

Several quantities are easier to estimate by theoretical methods than by experiments. For example, it is hard by experiments to unambiguously decide whether a bound ligand is strained or not by a protein. With theoretical methods, it is quite simple, since we can obtain the optimal structure of the isolated ligand, and therefore directly estimate the effect of strain (in geometry or energy) by comparing the structure and energy with the structure in the protein. We can even estimate the free energy cost for the protein to bind a certain ligand [54].

Generally speaking, it is often easier to obtain *energies* by theoretical methods than by experiments. This is a great advantage, since chemical processes are governed by energies. Therefore, theoretical methods can directly study reaction mechanisms, by obtaining reaction and activation energies, whereas experimental investigations mostly give indirect evidence that must be interpreted in terms of structures and energies. Moreover, technical problems, e.g. if the molecule of interest is spectroscopically invisible, short-lived, or hazardous, provide no hinder for theoretical chemistry; any molecule can be studied in the computer as long as you wish.

An illustrative example of the advantage of theoretical methods is the Cu–S_{Met} bond in blue copper proteins. It is the only bond that shows a clear variation among different crystal structure (i.e. an experimentally discernible variation). Therefore, it has been suggested to be important for the geometry and reduction potential of the proteins [13,112,116,118,119]. However, a large variation does not necessarily imply a functional importance. Our calculations show that it is instead caused by the flat potential surface (a small force constant) [35]. Thus, the large variation in bond length corresponds to a small variation in energy, and therefore the bond has a minor influence on the structure and function of the copper site.

In conclusion, we have shown that theoretical calculations can be used to successfully solve biochemical problems. In similarity with experimental methods, they involve assumptions and interpretation, and they have their limitations, but there are many problems that are best studied by theory. Thus, theoretical meth-

ods have become a competitive alternative to experiments for biochemical investigations.

REFERENCES

1. A.G. Sykes, Adv. Inorg. Chem. 36 (1990) 377.
2. T. Adman, Adv. Prot. Chem. 42 (1991) 145.
3. A. Messerschmidt, Struct. Bond. 90 (1998) 37.
4. J.M. Guss, H.D. Bartunik & H.C. Freeman, Acta Cryst. B48 (1992) 790.
5. W.E.B. Shepard, B.F. Anderson, D.A. Lewandoski, G.E. Norris & E.N. Baker J. Am. Chem. Soc. 112 (1990) 7817.
6. R.A. Marcus & N. Sutin, Biochim. Biophys. Acta 811 (1985) 265.
7. R.J.P. Williams (1963) in Molecular basis of enzyme action and inhibition (P.A.E. Desnuelle, ed), p. 133, Pergamon Press, Oxford.
8. B.G. Malmström (1965) in Oxidases and related redox systems (T.E. King, H.S. Mason, M. Morrison, eds.), vol. 1, p. 207, Wiley, New York.
9. B.L. Vallee & R.J.P. Williams, Proc. Natl. Acad. Sci. USA 59 (1968) 498.
10. R.J.P. Williams Eur. J. Biochem. 234 (1995) 363.
11. H.B. Gray & B.G. Malmström, Comments Inorg. Chem. 2 (1983) 203.
12. Malmström BG (1994) Eur. J. Biochem. 223 711.
13. J.A. Guckert, M.D. Lowery & E.I. Solomon, J. Am. Chem. Soc. 117 (1995) 2817.
14. U. Ryde, M.H.M. Olsson , K. Pierloot, B.O. Roos, J. Mol. Biol. 261 (1996) 586.
15. J.E. Rice, H. Horn, B.H. Lengsfiels, A.D. McLean, J.T. Carter, E.S. Replogle, L.A. Barnes, S.A. Maluendes, G.C. Lie, M. Gutwski, W.E. Rude, S.P.A. Sauer, R. Lindh, K. Andersson, T.S. Chevalier, P.-O.Widmark, D. Bouzida, G. Pacansky, K. Singh, C.J. Gillan, P. Carnevali, W.C. Swope & B. Liu (1995). Mulliken™ Version 2.25b, internal release, IBM Corporation, Almaden, USA.
16. D. Treutler & R. Ahlrichs J. Chem. Phys. 102 (1995) 346.
17. M.J. Frisch, G.W. Trucks, H.B. Schlegel, G.E. Scuseria, M.A. Robb J.R. Cheeseman, V.G. Zakrzewski J.A. Montgomery R.E. Stratmann, J.C. Burant, S. Dapprich, J.M. Millam, A.D. Daniels, K.N. Knudin, M.C, Strain, O. Farkas, J. Tomasi, V. Barone, M. Cossi, R. Cammi, B. Mennucci, C. Pomelli, C. Adamo, S. Clifford, J. Ochterski, G.A. Petersson, P.Y. Ayala, Q. Cui, K. , Morokuma, D.K. Malick, A.D. Rabuck, K. Raghavachari, J.B. Foresman, J. Cioslowski, J.V. Ortiz, B.B. Stefanov, G. Liu, A. Liashenko, P. Piskorz, I. Komaromi, R.Gomperts, R.L. Martin, D.J. Fox, T. Keith, M.A. Al-Laham, C.Y. Peng, A. Nanayakkara, C. Gonzalez, M. Challacombe, P.M.W. Gill, B.G. Johnson, W. Chen, M.W. Wong, J.L. Andres, M. Head-Gordon, E.S. Replogle & J.A. Pople 1998. Gaussian 98, Revision A.5, Gaussian, Inc, Pittsburgh PA.
18. R.H. Hertwig & W. Koch, Chem. Phys. Lett. 268 (1997) 345.
19. A. Ricca & C.W. Bauschlicher, J. Phys. Chem. 98 (1994) 12899.
20. A. Ricca & C. W. Bauschlicher, Theor. Chim. Acta 92 (1995) 123.
21. M. C. Holthausen, M. Mohr & W. Koch, Chem. Phys. Lett. 240 (1995) 245.
22. C.W. Bauschlicher, Chem. Phys. Lett. 246 (1995) 40.
23. A. Schäfer, H. Horn & R.J. Ahlrichs, Chem. Phys. 97 (1992) 2571.
24. E. Sigfridsson, M.H.M. Olsson & U. Ryde (2000) “A comparison of the inner-sphere reorganisation energies of cytochromes, iron–sulphur clusters, and blue copper proteins”, J. Mol. Biol. submitted.

25. W.J. Hehre, L. Radom, P.v.R. Schleyer & J.A. Pople, (1986) Ab initio molecular orbital theory, Wiley-Interscience, New York.
26. U. Ryde & M.H.M. Olsson (2000) "Accurate geometry optimisations of blue-copper models in vacuum, solvent, and the protein", J. Phys. Chem., submitted.
27. K. Andersson, P.-Å. Malmqvist, B.O. Roos, J. Chem. Phys. 96 (1992) 1218.
28. B.O. Roos, K. Andersson, M.P. Fülscher, P.-Å. Malmqvist, L. Serrano-Andrés, K. Pierloot & M. Merchán, in Advances in chemical physics New methods in coputatioal quantum mechanics (I. Prigogine & S.A. Rice eds.) 43 (1996) 219, John Wiley & Sons, New York.
29. K. Pierloot, B. Dumez, P.-O. Widmark & B.O. Roos, Theoret. Chim. Acta 90 (1995) 87.
30. B.O. Roos, K. Andersson, M.P. Fülscher, L. Serrano-Andrés, K. Pierloot, M. Merchán & V. Molina, J. Mol. Struct. 388 (1996) 257.
31. P-Å. Malmqvist & B.O. Roos, Chem. Phys. Lett, 245 (1989) 189.
32. K. Andersson, M.R.A. Blomberg, M.P. Fülscher, G. Karlström, R. Lindh, P.-Å. Malmqvist, P. Neogrády, J. Olsen, B.O. Roos, A.J. Sadlej, M. Schütz, L. Seijo, L. Serrano-Andrés, P.E.M. Sigebahn & P.-O. Widmark, (1997) MOLCAS version 4. University of Lund, Sweden.
33. J.O.A. De Kerpel, K. Pierloot, U. Ryde & B.O. Roos, J. Phys. Chem. B 102 (1998) 4638.
34. K. Pierloot, J.O.A. De Kerpel, U. Ryde, M.H.M. Olsson, B.O. Roos J. Am. Chem. Soc. 120 (1998) 13156.
35. M.H.M. Olsson &U. Ryde, J. Biol. Inorg. Chem. 4 (1999) 654.
36. K. Pierloot, J.O.A. De Kerpel, U. Ryde & B.O. Roos J. Am. Chem. Soc. 119 (1997) 218.
37. J.O.A. De Kerpel, K. Pierloot & U. Ryde J. Phys. Chem. B 103 (1999) 8375.
38. U. Ryde, M.H.M. Olsson, Roos BO, K. Pierloot & J.O.A. De Kerpel (1998) in The Encyclypaedia of Computational Chemistry, P.v.R. Schleyer, N.L. Allinger, T. Clark, J. Gasteiger, P.A. Kollman, H.F. Schaefer III & P.R. Schreiner (eds), John Wiley & Sons, Chichester, p. 2255.
39. A. Borin-Carlos, M.H.M. Olsson, U. Ryde, B.O. Roos, E. Cedergren-Zeppesauer & A. Merli (2000) "A theoretical study of the structure and electronic spectrum of Cu-substituted alcohol dehydrogenase", J. Am. Chem. Soc. submitted.
40. D.A. Case, D.A. Pearlman, J.W. Cadwell, T.E. Cheatham III, W.S. Ross, C.L. Simmering, T.A. Darden, K.M. Merz, R.V. Stanton, A. L. Cheng, J.J. Vincent, M. Crowley, D.M. Ferguson, R.J. Radmer, G.L. Seibel, U.C. Sing, P.K. Weinter, P.A. Kollman (1997) Amber 5.0, University of California, San Francisco.
41. J. Tomasi & M. Persico, Chem. Rev. (1994) 2027.
42. F.M. Floris, J. Tomasi & J.L. Pascal-Ahuir, J. Comput. Chem. 12 (1991) 784.
43. V. Barone & M. Cossi, J. Phys. Chem. A 102 (1998) 1995.
44. J.B. Foresman, T.A. Keith, K.B. Wiberg, J. Snoonian & M.J. Frisch, J. Chem. Phys. 100 (1996) 16098.
45. M.H.M. Olsson & U. Ryde (2000) "A theoretical study of the reduction potential of blue copper proteins", manuscript in preparation.
46. E. Sigfridsson & U. Ryde, J. Comput. Chem. 19 (1998) 377.
47. B. Honig, Science 268 (1995) 1144.
48. D. Bachford, Lecture notes in Computer Science 1343 (1997) 233.
49. U. Ryde, M.H.M. Olsson, B.O Roos, J.O.A. De Kerpel & K. Pierloot (2000) "On the role of strain in blue copper proteins", J. Biol. Inorg. Chem, in press.

50. A. Warshel (1991) Computer modelling of chemical reactions in enzymes and solutions, p. 209, J. Wiley, Sons, New York.
51. A.K. Churg, R.M. Weiss, A. Warshel & T. Takano, J. Phys. Chem. 87 (1983) 1683.
52. P.J. Stephens, D.R. Jollie & A. Warshel, Chem. Rev. 96 (1996) 2491.
53. C.A.P. Libeu, M. Kukimoto, M. Nishiyama, S. Hornouchi & E.T. Adman, Biochemistry, 36 (1997) 13160.
54. J.O.A. De Kerplel & U. Ryde, Prot. Struct, Funct, Genet, 36 (1998) 157.
55. A. Warshel & M. Karplus, J. Am. Chem. Soc. 94 (1972) 5612.
56. U.C. Singh & P.A. Kollman, J. Comp. Chem.7 (1986) 718.
57. U. Ryde, J. Comp.-Aided. Mol. Design. 10 (1996) 153.
58. M. Svensson, S. Humbel, R.D.J. Froese, T. Matsubara, S. Sieber, K. Morokuma, J. Phys. Chem. 100 (1996) 19357.
59. K.P. Eurenius, D.C. Chatfield, B.R. Brooks, Int. J. Quant. Chem. 60 (1996) 1189.
60. M.L. Field (1998) in the encyclypaedia of computational chemistry, P.v.R. Schleyer, N.L. Allinger, T. Clark, J. Gasteiger, P.A. Kollman, H.F. Schaefer III & P.R. Schreiner (eds.), John Wiley & Sons, Chichester 2255.
61. U. Ryde, J.O.A. De Kerpel, K. Pierloot & M.H.M. Olsson (2000) "The structure, spectroscopy, and reorganisation energy of azurin", manuscript in preparation.
62. N. Bonander, T. Vänngård, L.-C. Tsai, V. Langer, H. Nar & L. Sjölin, Proteins, Struct. Funct. Genet. 27 (1997) 385.
63. H.B. Gray, R.J.P. Williams & B.G. Malmström (2000) "Copper coordination in blue proteins", J. Biol. Inorg. Chem., in press.
64. F.A. Cotton & G. Wilkinson (1988) Advanced inorganic chemistry, Wiley, New York.
65. M.H.M. Olsson, U. Ryde, B.O. Roos & K. Pierloot, J. Biol. Inorg. Chem. 3 (1998) 109.
66. N. Kitajima, Adv. Inorg. Chem, 39 (1992) 1.
67. S. Mandal, G. Das, R. Singh, R. Shukla & P.K. Bharadwaj, Coord. Chem. Rev 160 (1997) 191.
68. M.H.M. Olsson, U. Ryde & B.O. Roos, Prot. Sci. 7 (1998) 2659.
69. S. Al-Karadaghi, E. Cedergren-Zeppesauer, Z. Dauter & K.S. Wilson, Acta Crystallogr. D51 (1995) 805.
70. A. Schäfer, C. Huber & R. Ahlrichs, J. Chem. Phys, 100 (1994) 5829.
71. A.D. Becke, Phys. Rev. A 38 (1988) 3098.
72. J.P. Perdew, Phys. Rev. B 33 (1986) 8822.
73. K. Eichkorn O. Treutler, H. Öhm, M. Häser & R. Ahlrihs, Chem. Phys. Lett. 240 (1995) 283.
74. J.M. Guss, P.R. Harrowell, M. Murata, V.A. Norris & H.C. Freeman, J. Mol. Biol. 192 (1986) 361.
75. U. Ryde, Prot. Sci. 4 (1995) 1124.
76. U. Ryde, Eur. J. Biophys. 24 (1996) 213.
77. U. Ryde & L. Hemmingsen, J. Biol. Inorg. Chem. 2 (1997) 567.
78. A.B.P. Lever, Inorganic electronic spectroscopy (1984), pp. 58-66, Elsevier, Amsterdam.
79. J. Han, T.M. Loehr, Y. Lu, J.S. Valentine, B.A. Averill & J. Sanders-Loehr, J. Am. Chem. Soc. 115 (1993) 4256.
80. Y. Lu, J.A. Roe, E.B. Gralla & J.S. Valentine, in Bioinorganic chemistry of copper, eds. K.D. Karlin & Z. Tyeklár, Chapman & Hall, New York (1993), p. 64.
81. C.R. Andrew, H. Yeom, J.S. Valentine, B.G. Karlsson, N. Bonander, G. van Pouderoyen, G.W. Canter, T. M. Loehr & J. Sanders-Loehr, J. Am. Chem. Soc. 116 (1994) 11489.

82. S.J. Kroes, C.W.G. Hoitink, C.R. Andrew, J.Y. Ai, J. Sanders-Loehr, A. Messerschmidt, W.R. Hagen & G.W. Canters, Eur. J. Biochem. 240 (1996) 342.
83. K.W. Penfield, A.A. Gewirth & E.I. Solomon, J. Am. Chem. Soc. 107 (1985) 4519.
84. A.A. Gewirth & E.I. Solomon, J. Am. Chem. Soc. 110 (1988) 3811.
85. L.B. LaCroix, S.E. Shadle, Y. Wang, B.A. Averill, B. Hedman, K.O. Hodgson, E.I. Solomon, J. Am. Chem. Soc. 118 (1996) 7755.
86. L.B. LaCroix, .D.W. Randall, A.M. Nersissian, C.W.G. Hoitink, G.W. Canters, J.S. Valentine & E.I. Solomon, J. Am. Chem. Soc. 120 (1998) 9621.
87. J. Sanders-Loehr, in Bioinorganic chemistry of copper, eds. K.D. Karlin & Z. Tyeklár, Chapman & Hall, New York (1993), pp. 51.
88. E.T. Adman, J.W.Godden & S. Turley, J. Biol. Chem. 270 (1995) 27458.
89. K.K. Stavrev & M. Zerner, Int. J. Quant. Chem. Quantum. Biol. Symp. 22 (1995) 155.
90. B.S. Brunschwig, S. Ehrenson & N. Sutin, J. Phys. Chem. 91 (1987) 4714.
91. Z. Zhou & S.U.M. Kahn, J. Phys. Chem. 93 (1989) 5292.
92. G. King & A. Warshel, J. Chem. Phys. 93 (1990) 8682.
93. C. Zheng, J.A. McCammon & P.G. Wolynes, Chem. Phys. 158 (1991) 261.
94. Y. Bu, S. Liu & X. Song, Chem. Phys. Lett, 227 (1994) 121.
95. H.-X. Zhou, J. Am. Chem. Soc. 116 (1994) 10362.
96. S. Larsson, A. Broo & L. Sjölin, J. Phys. Chem. 99 (1995) 4860.
97. I. Muegge, P.X. Qi, A.J. Wand, Z.T. Chu & A. Warshel, J. Phys. Chem. B 101 (1997) 825.
98. Y. Bu, Y. Ding, F. He, L. Jiang & X. Song, Internat. J. Quant. Chem. 61 (1997) 117.
99. G.M. Soriano, W.A. Cramer & L.I. Krishtalik, Biopys J. 73 (1997) 265.
100. K.A. Sharp, Biophys. J. 73 (1998) 1241.
101. Y.I. Kharkats & J. Ulstrup, Chem. Phys. Lett. 202 (1999) 320.
102. K. Sigfridsson, M. Sundahl, M.J. Bjerrum & Ö. Hansson, J. Biol. Inorg. Chem. 1 (1996) 405.
103. O. Farver & I. Pecht, Biophys Chem. 50 (1994) 203.
104. O. Farver, L.K. Skov, G. Gilardi, G. van Puderoyden & G.W. Canters, Chem. Phys. 204 (1996) 271.
105. J.R. Winkler, P. Wittung-Stafshede, J. Leckner, B.G. Malmström & H.B. Gray, Proc. Natl. Acad. Sci. USA 94 (1997) 4246.
106. A.J. Di Bilio, M.G. Hill, N. Bonander, B.G. Karlsson, R.M. Villahermosa, B.G. Malmström & H.B. Gray, J. Am. Chem. Soc. 119 (1997) 9921.
107. L.K. Skov, T. Pascher, J.R. Winkler & H.B. Gray, J. Am. Chem. Soc. 120 (1998) 1102.
108. F. Drepper, M. Hippler, W. Nitschke & W. Haehnel, Biochemistry 35 (1996) 1282.
109. G.R. Loppnow & E. Fraga, J. Am. Chem. Soc. 199 (1997) 896.
110. I. Zaitseva, V. Zaitsev, G. Card, K. Moshkov, B. Bax, A. Ralph & P. Lindley, J. Biol. Inorg. Chem. 1 (1996) 15.
111. T.E. Machonkin, H. H. Zhang, B. Hedman, K.O. Hodgson & E.I. Solomon, Biochem. 37 (1998) 9570.
112. R.H. Holm, P. Kennepohl & E.I. Solomon, Chem. Rev 96 (1996) 2239.
113. J.J.R. Fraústo da Silvia & R.P.J. Williams, The biological chemistry of the elements, Clarendon Press, Oxford, 1994.
114. H.-X. Zhou, J. Biol. Inorg. Chem. 2 (1997) 109.
115. B.R. James & R.P.J. Williams, J. Chem. Soc. (1961) 2007.
116. J. Leckner, P. Wittung, N. Bonander, B.G. Karlsson & B.G. Malmström, J. Biol. Inorg. Chem. 2 (1997) 368.

117. P. Wittung-Stafshede, M.G. Hill, E. Gomez, A.J. Di Bilio, B.G. Karlsson, J. Leckner, J.G. Winkler, H.B. Gray & B.G. Malmström, J. Biol. Inorg. Chem. 3 (1998) 367.
118. B.G. Malmström & J. Leckner, Curr. Op. Chem. Biol. 2 (1998) 286.
119. E.I. Solomon, K.W. Penfield, A.A. Gewirth, M.D. Lowery, S.E. Shadle, J.A. Guckert & L.B. Lacroix, Inorg. Chim Acta 243 (1996) 67.
120. T. Pascher, G. Karlström, M. Nordling, B.G. Malmström & T. Vänngård, Eur. J. Biochem. 212 (1993) 289.
121. B.G. Karlsson, L.-C. Tsai, H. Nar, J. Sanders-Loehr, N. Bonander, V. Langer & L. Sjölin, Biochemistry 36 (1997) 4089.
122. E.R. Dockal, T.E. Jones, W.F. Sokol, R.J. Engerer, D.B. Rorabacher & L.A. Ochrymowycz, J. Am. Chem. Soc. 98 (1976) 4322.
123. K.A. Sharp, Annu. Rev. Biophys. Biophys. Chem. 19 (1990) 301.
124. K.K. Rodgers & S.G. Sligar, J. Am. Chem. Soc. 113 (1991) 9419.
125. F.A. Tezcan, J.R. Winkler & H.B. Gray, J. Am. Chem. Soc. 120 (1998) 13383.
126. M.V. Botuyan, A. Toy-Palmer, J. Chung, R. C. Blake, P. Beroza, D.A. Case & H.J. Dyson, J. Mol. Biol. 263 (1996) 752.
127. G.T. Babcock & M. Wikström, Nature 356 (1992) 301.
128. S. Iwata, C. Ostermeier, B. Ludwig & H. Michel, Nature 376 (1995) 660.
129. M. Wilmanns, P. Lappalainen, M. Kelly, E. Sauer-Eriksson & M. Saraste, Proc. Natl. Acad. Sci. 92 (1995) 11955.
130. T. Tsukihara, H. Aoyama, E. Yamashita, T. Tomizaki, H. Yamaguchi, K. Shinzawa-Itoh, R. Nakashima, R. Yaono & S. Yoshikawa, Science 269 (1995) 1069.
131. B.G. Malmström & R. Aasa, Eur. J. Biochem. 325 (1993) 49.
132. H. Beinert, Eur. J. Biochem. 245 (1997) 521.
133. N.J. Blackburn, S. de Vries, M.E. Barr, R.P. Houser, W.B. Tolman, D. Sanders & J.A. Fee, J. Am. Chem. Soc. 119 (1997) 6135.
134. N.J. Blackburn,, M.E. Barr, W.H. Woodruff, J. van der Oost & S. de Vries, Biochem. 33 (1994) 10401.
135. S.E. Wallace-Williams, C.A. James, S. de Vries, M. Saraste, P. Lappalainen, J. van der Oost, M. Fabian, G. Palmer & W.H. Woodruff, J. Am. Chem. Soc. 118 (1996) 3986.
136. D.R. Gamelin, D.W. Randall, M.T. Hay, R.P. Houser, T.C. Mulder, G.W. Canters, S. de Vries, W.B. Tolman, Y. Lu & E.I. Solomon J. Am. Chem. Soc. 120 (1998) 5246.
137. P.M.H. Kroneck, W.E. Antholine, D.H.W. Kastrau, G. Buse, G.C.M. Steffens & W.G. Zumft, FEBS Lett. 268 (1990) 274.
138. F. Neese, W.G. Zumft, W.E. Antholine & P.M.H. Kroneck, J. Am. Chem. Soc. 118 (1996) 8692.
139. J.A. Farrar, F. Neese, P. Lappalainen, P.M.H. Kroneck, M. Saraste, W.G. Zumft & A.J. Thomson, J. Am. Chem. Soc. 118 (1996) 11501.
140. M. Karpefors, C.E. Slutter, J.A. Fee, R. Aasa, B. Källebring, S. Larsson & T. Vänngård, Biophys. J. 71 (1996) 2823.
141. K.R. Williams, D.R. Gmelin, L.B. LaCroix, R.P. Houser, W.B. Tolman, T.C. Mulder, S. de Vries, B. Hedman, K.O. Hodgson & E.I. Solomon, J. Am. Chem. Soc. 119 (1997) 613.
142. J.A. Farrar, R. Grinter, F. Neese, J. Nelson & W.H. Thompson, J. Chem. Soc., Datlon. Trans. (1997) 4083.
143. F. Neese, R. Kappl, J. Hüttermann, W.G. Zumft & P.M.H. Kroneck, J. Biol. Inorg. Chem. 3 (1998) 53.
144. S. Larsson (2000) “Evolution of energy saving electron pathways in proteins” J. Biol. Inorg. Chem. in press.

145. R.P. Houser, V.G. Young & W.B. Tolman, J. Am. Chem. Soc. 118 (1996) 2101.
146. J.A. Farrar, W.G. Zumft & A.J. Thomson, Proc. Natl. Acad. Sci. USA 95 (1998) 9891. J.A. Farrar, W.G. Zumft & A.J. Thomson, "Dimeric Copper Centres – from Cu_A to Cu_Z" J. Biol. Inorg. Chem. (2000) in press.
147. M.H.M. Olsson & U. Ryde (2000) "Geometry, reduction potential, and reorganisation energy of the binuclear Cu_A site studied by theoretical methods", Proc. Natl. Acad. Sci. USA, submitted.
148. C. Ostermeier, A. Harrenga, U. Ermler & H. Michel, Proc. Natl. Acad. Sci. USA 94 (1997) 10547.
149. S. Yoshikawa, K. Shinzawa-Itoh, R. Nakashima, R. Yaono, E. Yamashita, N. Inoue, M.J. Fei, C.P. Libeu, T. Mizushima, H. Yamaguchi, T. Tomizaki & T. Tsukihara, Science 280 (1998) 280.
150. P.A. Williams, N.J. Blackburn, D. Sanders, H. Bellamy, E.A. Stura, J.A. Fee & D.A. McRee, Nature Struct. Biol. 6 (1999) 509.
151. G. Henkel, A. Müller,S. Weissgräber, G. Buse, T. Soulimane, G.C.M. Steffens & H.-F. Nolting, Angew. Chem. Int. Ed. 34 (1995) 1489.
152. R.P. Houser, J.A. Halfen, V.G. Young, N.J. Blackburn & W.B. Tolman, J. Am. Chem. Soc. 117 (1995) 10745.
153. J.A. Farrar, P. Lappalainen, W.G. Zumft, M. Saraste & A.J. Thomson, Eur. J. Biochem. 232 (1995) 303.
154. M. Kelly, P. Lappalainen, G. Talbo, T. Halitia, J. van der Oost & M. Saraste, J. Biol. Chem. 268 (1993) 16781.
155. D.W.Randall, D.R. Gamelin, L.B. LaCroix & E.I. Solomon, J. Biol. Inorg. Chem. "Electronic structure contributions to electron transfer in blue copper proteins and Cu_A, in press.
156. S. Larsson, B. Källebring, P. Wittung & B.G. Malmström, Proc. Natl. Acad. Sci. USA 92 (1995) 7167.
157. B.E. Ramirez, B.G. Malmström, R.J. Winkler & H.B. Gray, Proc. Natl. Acad. Sci. USA 92 (1995) 11949.
158. P. Brzezinkski, Biochem. 35 (1996) 5611.
159. K.R. Hoke, C.N. Kiser, A.J. di Bilio, J.R. Winkler, J.H. Richards & H.B. Gray, J. Inorg. Biochem. 74 (1999) 165.
160. J.A. Farrar, W.G. Zumft & A.J. Thomson, Proc. Natl. Acad. Sci. USA 95 (1998) 9891.
161. J.A. Cowan, Inorganic biochemistry, an introduction, Wiley-VCH, New York, 1997.
162. S.J. Lippard & J.M. Berg, Principles of bioinorganic chemistry (1994) University Science Books, Mill Valley.
163. G. Palmer & J. Reedijk, Eur. J. Biochem. 200(1991) 599.
164. A.K. Churg & A. Warshel, Biochemistry 25 (1986) 1675.
165. Barkigia, K. M. J. Am. Chem. Soc. 110 (1988) 7566.
166. K.K.Rodgers & S.G. Sligar, J. Am. Chem. Soc. 113 (1991) 9419.
167. M.R. Gunner & B. Honig, Proc. Natl. Acad. Sci. USA 88 (1991) 9151.
168. R. Langen, Warshel, A. J. Mol. Biol. 224 (1992) 589.
169. M.R. Gunner, E. Alexov, E. Torres & S. Lipovaca, J. Inorg. Biol. Chem. 2 (1997) 126.
170. A. Warshel, J. Biol. Inorg. Chem. 2 (1997) 143.
171. P.J. Martel, J. Biol. Inorg. Chem. 4 (1999) 73.
172. R.K. Gupta, Biochim. Biophys. Acta 292 (1973) 291.
173. D.G. Nocera, J.R. Winkler, K.M. Yocom, E. Bordignon & H.B. Gray, J. Am. Chem. Soc. 106 (1984) 5145.

174. D.W. Dixon, X. Hong, S.E. Woehler, A.G. Mauk & B.P. Sishta, J. Am. Chem. Soc. 112 (1990) 1082.
175. F. Frolow, A.J. Smith, J.R. Guest & P.M. Harrison, Nature, Struct. Biol. 1 (1994) 453.
176. S.C. Baker, N.F.W. Saunders, A.C. Willis, S.J. Ferguson, J. Hajdu & V. Fülöp, J. Mol. Biol. 269 (1997) 440.
177. W.R. Scheidt, Acc. Chem. Res. 10 (1977) 339.
178. W.R. Scheidt & C.A. Reed, Chem. Rev. 81 (1981) 543.
179. D.W. Cruickshank, Acta Crystallogr. D55 (1999) 583.
180. J.E. Newton & M.B. Hall, Inorg. Chem. 23 (1996) 4627.
181. H. Beinert, R.H. Holm & E. Münck, Science 277 (1997) 653.
182. J.G. Norman & S.C. Jackels, J. Am. Chem. Soc. 97 (1975) 3833.
183. R.A. Bair & W.A. Goddard, J. Am. Chem. Soc. 100 (1978) 5669.
184. G.M. Jensen, A. Warshel, P.J. Stephens, Biochem. 33 (1994) 10911.
185. R.P. Christen, S.I. Spyros & E.T. Smith, J. Biol. Inorg. Chem. 1 (1996) 515.
186. P.D. Swartz, B.W. Beck & T. Ichiye, Biophys. J. 71 (1996) 2958.
187. P.D. Swartz & T. Ichiye, Biophys. J. 73 (1997) 2733.
188. I. Bertini, J. Biol. Inorg. Chem. 2 (1997) 114.
189. K.K. Stavrev, Int. J. Quant. Chem. 63 (1997) 781.
190. E.L. Bominaar, C. Achim, S.A. Borshch, J.-J. Girerd & E. Münck, Inorg. Chem. 36 (1997) 3689.
191. M. Czerwinski, Intern. J. Quant. Chem. 72 (1999) 39.
192. L. Noodleman & E.J. Baerends, J. Am. Chem. Soc. 106 (1984) 2316.
193. L. Noodleman, J.G. Norman, J.H. Osborne, A. Aizman & D.A. Case, J. Am. Chem. Soc. 107 (1985) 3418.
194. J.-M. Mouesca, J.L. Chen, L. Noodleman, D. Bashford & D.A. Case, J. Am. Chem. Soc. 116 (1994) 11898.
195. J.-M. Mouesca, L. Noodleman & D.A. Case, Intern. J. Quant. Chem. Quant. Biol. Symp. 22 (1995) 95.
196. L. Noodleman, C.Y. Peng, D.A. Case & J.-M. Moesca, Coord. Chem. Rev. 144 (1995) 199.
197. L. Noodleman, J. Biol. Inorg. Chem. 1 (1996) 177.
198. L. Noodleman & D.A. Case, Adv. Inorg. Chem. 38 (1996) 423.
199. R.W. Lane, J.A. Ibers, R.B. Rankel, G.C. Papaefthymiou & R.H. Holm, J. Am. Chem. Soc. 99 (1975) 84.i
200. R.G. Shulman, J. Mol. Biol. 124 (78) 305.
201. E.T. Adman, K.D. Waterpaugh & L.H. Jensen, Proc. Natl. Acad. Sci. USA 72 (1975) 4854.
202. Brookhaven protein data bank files 1cad, arb9, and 8rxn.
203. Brookhaven protein data bank files 1caa, 1dfx, 1rdg, 4rxn, 5rxn, and 6rxn.
204. J.J. Mayerle, S.E. Denmark, B.V.DePamphilis, J.A. Ibers & R.H. Holm, J. Am. Chem. Soc. 97 (1975)1032.
205. Brookhaven protein data bank files 1frd, 1frr, 1fxi, 1qt9, and 4fxc.
206. S. Iwata, M. Saynovits, T.A. Link & H. Michel, Structure 4 (1996) 567.
207. C.J. Carrell, H. Zhang, W.A. Cramer & J.L. Smith, Struct. 5 (1997) 1613.
208. M.D. Lowery, J.A. Guckert, M.S. Gebhard & E.I. Solomon, J. Am. Chem. Soc. 115 (1993) 3012.
209. R. Lumry & H. Eyring, J. Phys. Chem. 58 (1954) 110.
210. P. Ghosh, D. Shabat, K. Kumar, S.C. Sinha, F. Grynszpan, J. Li, L. Noodleman & E. Keinan, Nature, 382 (1996) 339.

211. T.L. Poulos, J. Biol. Inorg. Chem. 1 (1996) 356.
212. L. Stryer (1995) Biochemistry p. 218.
213. M. Levitt (1974) Peptides, polypeptides and proteins (E.R. Blout, F.A. Bovey, M. Goodman, N. Lotan, eds.), p. 99, Wiley, New York.
214. A. Fersht (1985) Enzyme Structure and Mechanisms, p. 341, W.H. Freeman & Co., New York.
215. J. Boström, P.-O. Norrby & T. Liljefors, J. Comp.-Aided Mol. Design. 12 (1998) 383.
216. A.A. Gewirth, S.L. Cohen, H.J. Schugar & E.I. Solomon, Inorg. Chem. 26 (1987) 1133.
217. W.B. Church, J.M. Guss, J.J. Potter & H.C. Freeman, J. Biol. Chem. 261 (1986) 234.
218. D. Barrick Curr. Opin. Biotechn. 6 (1995) 411.
219. H. Nar, A. Messerschmidt, R. Huber, M. van der Kamp & G.W. Canters, FEBS Lett. 306 (1992) 119.
220. T.P.J. Garrett, J.M. Guss, S.J. Rogers & H.C. Freeman, J. Biol. Chem. 259 (1984) 2822.
221. W.E.B. Shepard, R.L. Kingston, B.F. Anderson & E.N. Baker, Acta Cryst. D49 (1993) 331.
222. N. Kitajima, K. Fujisawa, M. Tanaka & Y. Moro-Oka, J. Am. Chem. Soc. 114 (1992) 9232.
223. P.L. Holland, W.B. Tolman, J. Am. Chem. Soc. 121 (1999) 7270.
224. H.W. Hellinga, J. Am. Chem. Soc, 120 (1998) 10055.
225. K. Nilsson, G. Kleywegt & U. Ryde (2000) “Quantum chemical refinement of crystal structures”, manuscript in preparation.